

MOLECULAR PROCESSES IN COMETS

Grant NAGW-1561

Annual Progress Report No. 5

For the period 1 November 1995 through 31 October 1996

009017

Principal Investigator

Dr. A. Dalgarno

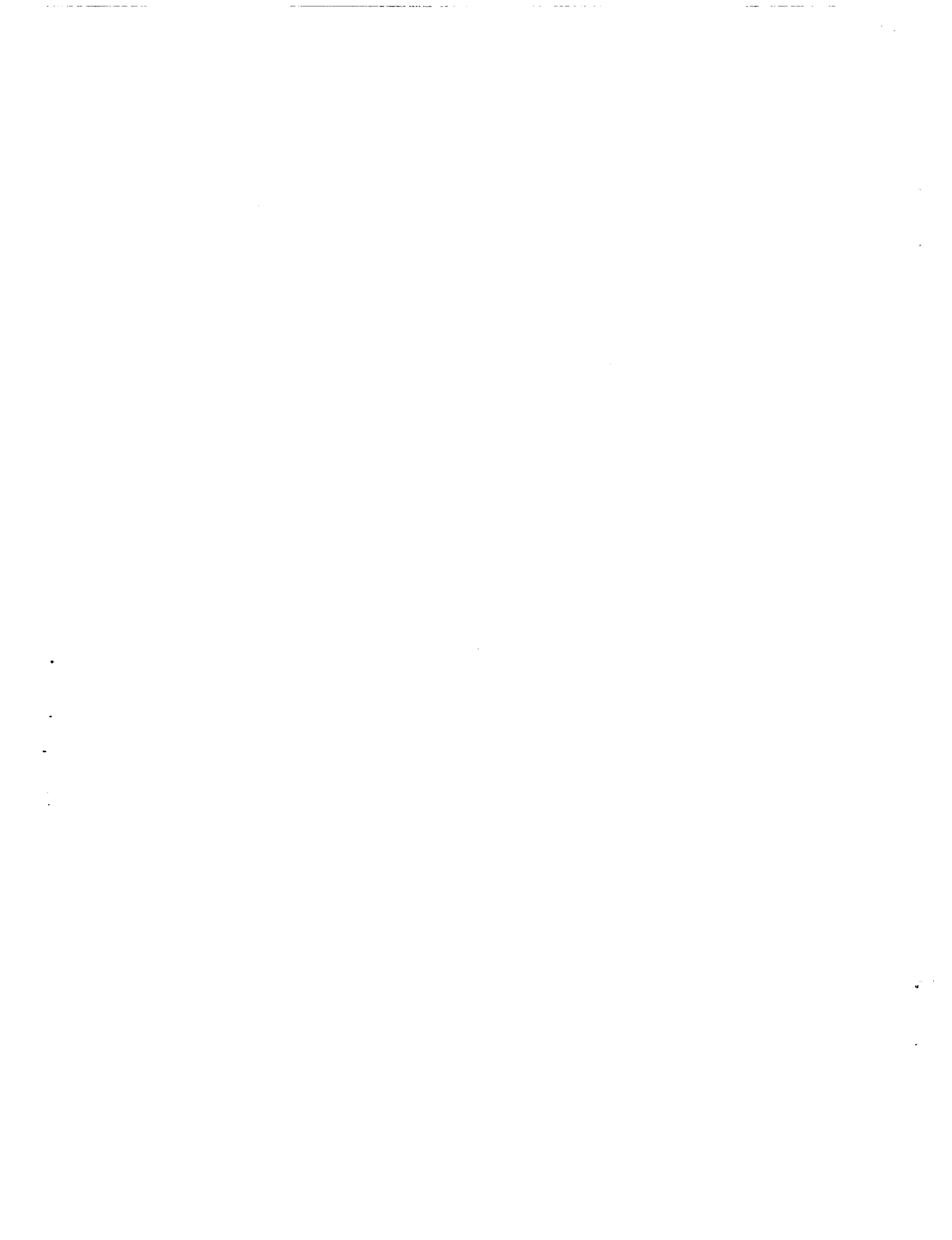
December 1996

Prepared for  
National Aeronautics and Space Administration  
Washington, D. C. 20546

Smithsonian Institution  
Astrophysical Observatory  
Cambridge, Massachusetts 02138

The Smithsonian Astrophysical Observatory  
is a member of the  
Harvard-Smithsonian Center for Astrophysics

The NASA Technical Officer for this grant is Dr. Jay Bergstrahl, Code EL,  
S1/Planetary Programs, NASA, Washington, D. C. 20546.



Molecular Processes in Comets

NAGW-1561

Annual Progress Report No. 5

For the period 1 November 1995 to 31 October 1996

We have been engaged in extensive semi-classical calculations of the rate coefficients for direct and exchange transitions between rovibrational levels of molecular hydrogen in collision with atomic hydrogen. Some results have appeared in the Astrophysical Journal Supplement 99, 345, 1995. The calculations have been completed for all possible transitions and the extensive material is being prepared for publication. The processes are important in the atmospheres of the Jovian planets and also in interstellar clouds subjected to cosmic rays, X-rays or ultraviolet photons. Dr. S. Tiné, who was partly supported by the grant, provided the rate coefficient data and they were used in a study of the infrared response of H<sub>2</sub> to X-rays in dense clouds. A paper has been submitted to the Astrophysical Journal. A copy is attached to this report.

Our investigation of the ultraviolet dayglow spectrum of the dayglow of Jupiter has been published in the Astrophysical Journal 462, 502-518, 1996. We also calculated the ultraviolet spectra of the Jovian aurora and concluded from a comparison with Hubble Space Telescope observations that the atmosphere has a large temperature gradient. The analysis has appeared in the Astrophysical Journal 467, 446-453, 1996.

## Papers

S. Lepp, V. Buch and A. Dalgarno, Collisional Excitation of H<sub>2</sub> Molecules by H Atoms, ApJS 98, 345 (1995).

W. Liu and A. Dalgarno, The Ultraviolet Spectra of the Jovian Dayglow, ApJ 462, 502 (1996).

W. Liu and A. Dalgarno, The Ultraviolet Spectra of the Jovian Aurora, ApJ 467, 446 (1996).

S. Tiné, S. Lepp, R. Gredel and A. Dalgarno, Infrared response of H<sub>2</sub> to X-rays in Dense Clouds, ApJ submitted (1996).

Submitted to *The Astrophysical Journal*

## Infrared response of H<sub>2</sub> to X-rays in dense clouds

S. Tiné and S. Lepp

Physics Dept., University of Nevada, Las Vegas, NV 89154-4002  
stefano@physics.unlv.edu, lepp@physics.unlv.edu

R. Gredel

European Southern Observatory, Casilla 19001, Santiago, Chile  
rgredel@eso.org

and

A. Dalgarno

Center for Astrophysics, 60 Garden Street, Cambridge, MA 02138  
adalgarno@cfa.harvard.edu

## ABSTRACT

The excitation by X-rays and cosmic rays of molecular hydrogen in interstellar clouds is analyzed. We carried out detailed calculations of entry efficiencies in rovibrational levels of H<sub>2</sub> following impact with fast electrons produced by X-ray ionization of the gas. The competing effect of collisional excitation, and quenching, by the ambient gas is examined in detail. Up to date values for H-H<sub>2</sub> collisional rate coefficients are adopted, and some derivations of H<sub>2</sub>-H<sub>2</sub> rovibrational rate coefficients from existing literature data are proposed. Several models as a function of temperature, density and ionization rate are presented. We found that H<sub>2</sub> infrared emission in X-ray dominated regions (XDR) is potentially observable for temperatures and ionization rates lower than certain critical values (typically  $T < 1000\text{K}$  and  $\zeta/n_{\text{H}} < 10^{-15} \text{ cm}^3 \text{ s}^{-1}$ , where  $\zeta$  is the ionization rate). At higher temperatures, collisional excitation by the ambient gas dominates the population of low vibrational levels, and at higher values of  $\zeta/n_{\text{H}}$  the abundance of H<sub>2</sub> is negligible. If such conditions are satisfied, the resulting infrared emission spectrum can be used as a diagnostic of nearby X-ray sources such as in cooling flows in galaxy clusters, quasars, Seyfert galaxies and supernova remnants. The intensity ratio of the 2-1S(1) and 1-0S(1) lines measured for the Seyfert galaxy NGC1275 is consistent with X-ray pumping.

*Subject headings:* ISM: molecules — X-rays: ISM — X-rays: galaxies — infrared: ISM: lines and bands — infrared: galaxies — galaxies: individual (NGC 1275)

## 1. Introduction

Emission lines from excited rotation-vibration levels of H<sub>2</sub> have been detected in a diverse range of objects in our galaxy and in external galaxies. The rotation-vibration levels may be excited in collisions in warm gas and the resulting spectrum is often invoked as an indicator that shocks are occurring. The levels may also be excited directly in the process of forming the molecules and they may be excited by a process of ultraviolet pumping. Yet another mechanism is initiated by cosmic rays or by X-rays. Lepp and McCray (1983) have pointed out that X-rays absorbed in a dense gas heat the gas so that thermal excitation of the rotation-vibration levels occurs. The X-ray photoelectrons may also produce excited rotation-vibration levels in a process analogous to ultraviolet pumping. Similar processes occur through the secondary electrons produced by cosmic ray ionization.

The photoelectrons and secondary electrons excite H<sub>2</sub> to singlet and triplet electronic states. The triplet states lead to dissociation but in some fraction of the excitations the singlet states cascade down by allowed radiation transitions into the array of rotation-vibration levels of the ground electronic state.

Gredel and Dalgarno (1995) have calculated the rates of populating individual ro-vibrational levels by fast electrons moving in a gas of molecular hydrogen but they did not include the effects of collision processes in the gas on the resulting emission spectrum. Here we have carried out calculations of the spectrum for different gas densities.

We have conducted a thorough review of the literature on the rate coefficients for H<sub>2</sub>-H<sub>2</sub> collisions and we have fitted their dependence on temperature by various formulas. The uncertainties are large. For H<sub>2</sub>-H collisions we use the results of the classical trajectory calculations of Lepp, Buch, and Dalgarno (1995) and Lepp, Tiné, and Dalgarno (1997).

The infrared emission spectrum can be determined from the calculated equilibrium populations for any given flux of fast electrons for any given distribution of hydrogen between its atomic and molecular forms and any given total hydrogen density. Some examples of the resulting spectra are presented and discussed.

## 2. Method

### 2.1. Entry rates

For each level (v,J) of the ground electronic state we have extended the calculations of Gredel and Dalgarno (1995) and determined the *entry efficiencies*  $\alpha(v,J)$  per unit molecule following impact with non-thermal electrons. The entry efficiencies per ionizing event do not vary much with the energy of the secondary electrons and we adopt the calculations of Gredel and Dalgarno (1995) for electrons with energy of 30eV. Due to the low temperatures of interstellar clouds,

the H<sub>2</sub> resides mostly in the ground vibrational level, in a distribution of rotational levels. The entry efficiencies corresponding to any given initial rotational distribution of H<sub>2</sub> can be accurately reproduced by weighting the response of individual rotational levels (Gredel and Dalgarno, 1995).

If  $\zeta$  is the total ionization rate in s<sup>-1</sup> due to X-rays or cosmic rays, then the entry rate (cm<sup>-3</sup> s<sup>-1</sup>) into level (v,J) due to electron impact excitations is given by:

$$X_{v=0,J} = \zeta n(\text{H}_2) \sum_{J_i \neq J} \chi_{J_i} \alpha_{J_i}(0, J)$$

$$X_{v>0,J} = \zeta n(\text{H}_2) \sum_{J_i} \chi_{J_i} \alpha_{J_i}(v, J)$$

where  $\chi_{J_i}$  is the fractional population of level J<sub>i</sub> in v=0.

For any initial rotational level J<sub>i</sub> (of v=0) the sum of the entry efficiencies to any other ro-vibrational level is equal to the number of exits from the initial level:

$$\beta_{J_i} = \text{net exit efficiency} = \sum'_{v,J} \alpha_{J_i}(v, J)$$

where the prime indicates that the re-entry into the initial level itself is excluded.

Analogously to the definition for entry rates, the net exit rate (cm<sup>-3</sup> s<sup>-1</sup>) out of level (v,J) is given by:

$$Y_{v=0,J} = \zeta n(\text{H}_2) \chi_J \beta_J$$

$$Y_{v>0,J} = 0.$$

## 2.2. Collisional rate coefficients

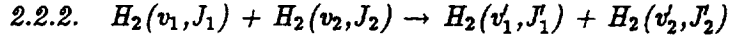
The important collisional partners of H<sub>2</sub> in interstellar space are H, He, H<sup>+</sup> and H<sub>2</sub>. The literature on the subject, especially regarding ro-vibrational transitions between high energy states, is sparse. Various empirical models have been used in previous calculations (Draine, Roberge, and Dalgarno 1983, Sternberg and Dalgarno 1989). We have reviewed the most recent literature and constructed the model described below for each type of collision process.

### 2.2.1. H<sub>2</sub>(v,J) + H → H<sub>2</sub>(v',J') + H

Recently, Lepp, Buch, and Dalgarno (1995) have published semi-classical calculations of rate coefficients Q<sub>H</sub>(v,J;v',J') at T=1000K by using the recent BKMP potential surface of Boothroyd

et al. (1991). Calculations at higher temperatures have been carried out and empirical fits for the temperature dependence for  $T \geq 1000\text{K}$  have been produced (Lepp, Tiné, and Dalgarno, 1997). In Fig. 1 the calculated rate coefficients (with error bars) and the adopted fits (dotted line) from Lepp, Tiné, and Dalgarno (1997) are presented for the two transitions  $(v=1, J=3) \rightarrow (v=1, J=1)$  and  $(v=1, J=3) \rightarrow (v=0, J=3)$ . Similar calculations have been reported by Martin and Mandy (1995) and a comparison with them is presented by Lepp, Tiné, and Dalgarno (1997).

For temperatures below 1000K the semi-classical approximation ceases to be valid. Quantum tunneling effects become a factor, particularly for non-reactive scatterings in which the ortho-para character of  $\text{H}_2$  is maintained. At 1000K, the semi-classical results of Lepp, Buch, and Dalgarno (1995) agree to within a factor of two with the quantum calculations of Sun and Dalgarno (1994), when the DMBE potential energy surface (Varandas et al. 1987) is used, and a factor of three with the quantum calculations of Flower and Wroe (1997) when the BKMP surface (Boothroyd et al. 1991) is used. For temperatures below 1000K we accounted for tunneling enhancement of pure rotational rate coefficients in  $v=0$  as described by Lepp, Tiné, and Dalgarno (1997).



For  $\text{H}_2\text{-H}_2$  collisions we distinguish pure rotational and ro-vibrational transitions. Pure rotational ( $v_1=v'_1$ ,  $v_2=v'_2$ ) rate coefficients are taken from the fits of Abgrall et al. (1992) to the original data of Danby, Flower, and Monteiro (1987) (strictly valid for  $v_1=v_2=0$ , here assumed to be valid for all  $v_1$ ,  $v_2$ ). Only transitions with  $|\Delta J_1|=2$  and  $\Delta J_2=0$  are considered. We also assume the rate coefficients for this type of transition to be independent of  $J_2$ . As an example, the rate coefficient for the case  $J_1 = 3 \rightarrow 1$  is presented in Fig. 1 as a function of temperature.

For transitions with  $\Delta v_1 \neq 0$  and/or  $\Delta v_2 \neq 0$  we restrict ourselves to collisions in which at least one of the two  $\text{H}_2$  molecules is in the  $v=0$  state, either before or after the collision. All other transitions are disregarded due to the relatively small abundance of  $\text{H}_2(v>0)$  molecules. The rate coefficients  $Q_{\text{H}_2}(v_1, v'_1; v_2, v'_2)$  for VT transitions, involving exchange of energy between vibrational and translational modes, and VV transitions, involving an exchange of vibrational energies between the molecules, are derived as functions of  $v_1$ ,  $v_2$ ,  $v'_1$ ,  $v'_2$  and  $T$  from Cacciatore, Capitelli, and Billing (1989) and Cacciatore and Billing (1992), who presented values of  $Q_{\text{H}_2}(v, v-1; 0, 0)$  and  $Q_{\text{H}_2}(1, 0; v, v)$  for  $v>0$  and of  $Q_{\text{H}_2}(v, v-1; 0, 1)$  for  $v>1$ .

Kolesnick and Billing (1993) and Billing and Kolesnick (1993) have subsequently revised the results for  $Q_{\text{H}_2}(2, 1; 0, 1)$  using updated potential curves. Neither the later revisions nor the original results match well the experimental data at  $T=300\text{K}$  (Kreutz et al. 1988). We decided to scale the results of Billing and Kolesnick (1993) by a factor of 10 to intersect the experimental error bar at  $T=300\text{K}$ . For consistency, we have also adopted the same scaling by 10 for the other transitions of similar type. For the  $v=2$  case, we took into account the experimental result  $Q_{\text{H}_2} \sim 10^{-17} \text{ cm}^3 \text{ s}^{-1}$  at  $T=82\text{K}$  (Teitelbaum 1984).

We have fitted the results to the Arrhenius-type expression  $\log_{10}Q_{H_2}(T) = A - B/T + C\log_{10}T$  with the constraint  $B > 0$  as did Lepp, Tiné, and Dalgarno (1997) for the  $H_2$ -H collisional rate coefficients. The coefficients A, B and C are presented in Table 1. For  $Q_{H_2}(v,v-1;0,0)$  we have held  $B=20$  for all  $v>1$ , to mimic the result for the case  $v=1$  for which more information is available about the temperature dependence (Cacciatore et al. 1989); for all other cases, except only  $v=7$ , a direct fitting would result in negative B coefficients, which yield unacceptable rate coefficients at low temperatures. All the fits reproduce the original results with a maximum deviation of 1%, except for  $Q_{H_2}(1,0;v,v)$  transitions where the deviation can be as high as 28%. However, these transitions are the least important among those listed.

The ro-vibrational transitions discussed above are single-quantum transitions in which the vibrational quantum numbers change at most by 1. For multi-quantum transitions there exist only some illustrative results for VV transitions (Cacciatore and Billing 1992). From these results we have arbitrarily assumed that the rate coefficients of all transition  $(v,v-1;0,1)$  may be scaled down by  $10^{1-k}$  when the first  $H_2$  molecule undergoes a transitions from  $v$  to  $v - k$ . We have assumed such a scaling applies also to the rate coefficients  $Q_{H_2}(v,v-k;0,0)$  and  $Q_{H_2}(k,0;v,v)$  of VT transitions.

The individual ro-vibrational rate coefficients have been derived from the formulas given above by assuming that only the three branches  $\Delta(J)=0, \pm 2$  are open and that they are of identical weight. Furthermore, we assumed that the rate coefficients averaged over initial rotational levels and summed over final ones reproduce the above band integrated values. For endothermic channels a factor equal to  $\exp(-E_{th}/kT)$ , where  $E_{th}$  is the energy threshold for the transitions, has been included. The resulting rate coefficients can be derived by Fortran subroutines publicly available on the World Wide Web (<http://www.physics.unlv.edu/astrophysics/>).

Fig. 1 shows the rate coefficients derived for the VT ro-vibrational de-excitation  $H_2(v=1,J=3) + H_2(0,0) \rightarrow H_2(0,1) + H_2(0,0)$ . The figure shows that the  $H_2$ - $H_2$  ro-vibrational de-excitation rate coefficients are two orders of magnitude smaller than similar rate coefficients for  $H_2$ -H collisions, while the rate coefficients for pure rotational transitions are of comparable magnitude.

### 2.2.3. $H_2(v,J) + He \rightarrow H_2(v',J') + He$

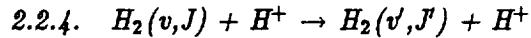
The  $H_2$ -He system has been widely studied due to its relative simplicity. For the rate coefficients reliable data for the pure rotational transitions (with  $v=0$ ) are available. We adopt here the calculations of Schaefer and Köler (1985) as fitted by Abgrall et al. (1992).

For transitions involving a change in the vibrational quantum number  $v$  of the colliding  $H_2$ , few data are available. For the  $v=1 \rightarrow 0$  transition experimental results by Audibert et al. (1976) are available at temperatures between 50 and 300K. We interpolated the data points using the fits:

$$Q_{He}(1;0)(T) = \begin{cases} 10^{-8.8T^{-1/3} - 16.5} & T \leq 90K \\ 10^{-18.9T^{-1/3} - 14.2} & 90K < T \leq 230K \\ 10^{-47.4T^{-1/3} - 9.4} & T > 230K \end{cases}$$

and we adopted these same rate coefficients for  $\Delta v=1$  transitions of higher vibrational levels. Extrapolating above 300K results in rate coefficients very similar to the H<sub>2</sub>-H<sub>2</sub> ones for the entire temperature range of interest (see Fig. 1, dashed lines). Since these rate coefficients are expected to be comparable on theoretical ground, the extrapolations are used in the model.

The ro-vibrational rate coefficients are then extracted following the procedure applied earlier to H<sub>2</sub>-H<sub>2</sub> collisions. For  $\Delta v \geq 2$ , we scaled the rate coefficients by  $10^{1-k}$  for the transitions v to v-k as for H<sub>2</sub>-H<sub>2</sub>.



Rate coefficients for pure rotational transitions in the ground vibrational state have been measured by Gerlich (1990) who presented a set of parameters for Arrhenius fits  $Q(J)=Q_0 e^{-\Delta E_0/kT}$  to the data. We adopted his fits for the exothermic channels and applied detailed balance to obtain the rate coefficients for the reverse transitions. Gerlich's fits included transitions from any initial rotational level  $J \leq 9$  to any lower lying rotational level in the temperature range  $10K \leq T \leq 500K$ . We have assumed his fits to be valid for higher temperatures also.

Transitions induced by proton impact are not significant in the molecular regions we explore except in bringing about ortho-para exchanges through proton interchange. For these exchanges, only those with  $\Delta J = \pm 1$  need be included. For their rate coefficients we used the following linear fits to the Arrhenius parameters of Gerlich (1990) as a function of J (with  $8 < J \leq 15$ ):

$$Q_0(J) = \begin{cases} -0.225J + 3.405 & \text{if } J=\text{odd} \\ -0.7745J + 11.04 & \text{if } J=\text{even} \end{cases}$$

$$\Delta E_0(J) = \begin{cases} 0.014J - 0.291 & \text{if } J=\text{odd} \\ 0.00835J - 0.189 & \text{if } J=\text{even} \end{cases}$$

For  $J > 15$ , we assume the rate coefficients equal to that for  $J=14 \rightarrow 13$  for even initial J and to that for  $J=15 \rightarrow 14$  for odd initial J.

### 2.3. Statistical equilibrium equations

In the present work we are interested in the effects of H<sub>2</sub> pumping by electron impact. Quenching by collisions with the ambient gas and radiative cascade are also included, but other competing processes such as formation and dissociation that could affect the resulting ro-vibrational distribution are neglected. The equations of statistical equilibrium may be written as follows:

$$0 = \frac{d\chi_{vJ}}{dt} = [\sum_{v'J'}(A_{v'J',vJ} + k_{v'J',vJ})\chi_{v'J'}] - \chi_{vJ}[\Gamma_{vJ} + \sum_{v'J'}k_{vJ,v'J'}] + \frac{(X_{vJ} - Y_{vJ})}{n(H_2)} \quad (1)$$

where

$$\begin{aligned} \Gamma_{vJ} &= \sum_{v'J'} A_{vJ,v'J'} \\ k_{vJ,v'J'} &= Q_H(vJ, v'J')n(H) + Q_{He}(vJ, v'J')n(He) + Q_{H+}(vJ, v'J')n(H^+) \\ &\quad + \sum_{v_2J_2, v'_2J'_2} Q_{H_2}(vJ, v'J'; v_2J_2, v'_2J'_2)\chi_{v_2J_2}n(H_2) \end{aligned} \quad (2)$$

The fractional abundances  $\chi_{v,J}$  have also to satisfy the conservation requirement  $\sum_{v,J}\chi_{v,J} = 1$ . Eqn. (2) must be modified for pure rotational transitions induced in H<sub>2</sub>-H<sub>2</sub> collisions by eliminating the sum over the quantum numbers of the second H<sub>2</sub> molecule and replacing the term  $\chi_{v_2,J_2}$  by 1.

We have solved the system of equations (1) for initial J values up to J=9. Electron pumping out of higher rotational levels is negligible for the temperatures and ionization fluxes we consider.

### 3. Results

The entry efficiencies from individual initial rotational levels have been calculated for different values of the fractional ionization of the gas. As pointed out by Gredel and Dalgarno (1995), with increasing fractional ionization of the gas more energy is transferred from the non-thermal electrons into the kinetic energy of the gas by elastic scattering with thermal electrons than to excitation of H<sub>2</sub>. In particular, the low energy collisions resulting in direct vibrational excitation of H<sub>2</sub> become rare with increasing fractional ionization. Therefore the excitation of v=1 and v=2 in low energy collisions diminishes for high values of the fractional ionization. Tables 2-5 show the calculated entry efficiencies  $\alpha_{J_i}(v, J)$  as a function of initial rotational level  $J_i \leq 9$  and final ro-vibrational levels (v,J), with increasing fractional ionization for the three branches  $\Delta J = J - J_i = 0, \pm 2$ . For an initial rotational distribution  $\omega_{J_i}$ , the effective entry rate into level (v,J) is given to a very good approximation by  $\sum_{J_i} \omega_{J_i} \alpha_{J_i}(v, J)$ . The tables show that electron pumping

enhances the populations of the vibrational levels but does not much alter the relative rotational populations of any given vibrational level. The ratios of the intensities of emission lines originating from the same vibrational level provide accordingly a measure of the initial rotational population. From it the kinetic temperature of the gas can be derived, provided that the excited rotational populations are not perturbed by other processes.

In presenting the infrared emission spectra arising from X-ray photoelectron pumping, we take as free parameters of the models the temperature, the density, and the ionization rate. We ignore pumping by any ultraviolet radiation field that may be present (Black and van Dishoeck 1987), assuming either that it is dominated everywhere by the X-rays or that its influence is limited to a narrow boundary of the molecular region of the cloud. To restrict the range of models we calculated the ratio  $n(\text{H})/n(\text{H}_2)$  of atomic and molecular hydrogen densities and the fractional ionization  $\epsilon(e) = n(e)/n_{\text{H}}$  following the procedures of Lepp and Dalgarno (1996). In all the models the helium abundance was held at  $n_{\text{He}}/n_{\text{H}} = 0.1$ . We limited  $(\zeta/n_{\text{H}})$  to less than  $10^{-15} \text{ cm}^3 \text{ s}^{-1}$ , for which the ionization ratios  $n(\text{H}^+)/n_{\text{H}}$  and  $n(\text{He})^+/n_{\text{He}}$  are about  $1.6 \times 10^{-2}$ . For  $(\zeta/n_{\text{H}})$  greater than  $10^{-15} \text{ cm}^3 \text{ s}^{-1}$ , vibrational energy transfers by electron and proton impacts modify the vibrational level populations. For  $\zeta/n_{\text{H}} = 10^{-15} \text{ cm}^3 \text{ s}^{-1}$  preliminary estimates indicate possible enhancements of up to a factor of two in the emissivities of the  $v=1 \rightarrow 0$  transitions. Reliable proton impact cross section data for vibrational transitions are not available. However, for high values of  $\zeta/n_{\text{H}}$  the abundance of  $\text{H}_2$  is small and the infrared emission is weak.

Excitation of the vibrational levels occurs by photoelectron collisions and by neutral particle collisions. Vibrational excitations in collisions with H are much more efficient than in collisions with  $\text{H}_2$  or with He and for  $(\zeta/n_{\text{H}}) = 10^{-17} \text{ cm}^3 \text{ s}^{-1}$ , neutral particle collisions are dominated by hydrogen atom impacts. Depopulation of the vibrational levels occurs by radiative decay at low densities and by neutral atom collisional quenching at high densities.

The level population is dominated by photoelectron collisions when the ionization rate exceeds some critical value, which occurs when the product of the ionization rate and the entry efficiency is equal to the rate at which collisions populate the level. If  $Q_{up}$  is the total effective rate coefficient at which collisions populate the level and  $\alpha$  is the total effective entry efficiency into the level then

$$(\zeta/n_{\text{H}})_{cr} = Q_{up}/\alpha \quad (3)$$

The effective rate coefficient and entry efficiency are calculated by summing over all possible population channels.

To illustrate the dependence of the emission spectrum on density and temperature, we present in Tables 6a, 6b and 6c the predicted emissivities  $\epsilon$  ( $\text{erg s}^{-1}$ ) per  $\text{H}_2$  molecule of a selection of  $\text{H}_2$  infrared emission lines for a gas at temperatures of 500K, 1000K and 2000K respectively at densities ranging up to  $10^7 \text{ cm}^{-3}$  subjected to ionizing fluxes such that  $(\zeta/n_{\text{H}}) = 10^{-17} \text{ cm}^3 \text{ s}^{-1}$ . Then  $n(\text{H})/n(\text{H}_2) = 1.9$  and  $n_e/n_{\text{H}} = 2 \times 10^{-5}$ .

At 500K, neutral particle collisions are inefficient in causing excitation and the levels are populated by photoelectron impact. The vibrational levels  $v=1$  and  $v=2$  are excited by direct electron impact excitation of the ground vibrational level and the higher  $v=5$  and  $v=6$  levels are excited by cascading from electronically excited states of  $H_2$ . The behavior of the  $v=5$  and 6 levels is characteristic of levels  $v \geq 3$ . The intensities of the emissions from high vibrational levels are much less than those of the  $v=1-0$  and  $2-1$  transitions. The marked difference in intensities is an indication of electron pumping and contrasts with that expected from ultraviolet pumping. The increase in line intensities with increasing  $n_H$  is a reflection of the increase in  $\zeta$  imposed by the assumption of a constant ( $\zeta/n_H$ ). The modifying influence of neutral particle collisions can be seen in the changing relative intensities of the  $1-0S(0)$ ,  $S(1)$  and  $S(2)$  lines and in the saturation of the intensities with increasing density.

At 1000K and 2000K, thermal collisions with H atoms occur rapidly and they play a major role in determining the vibrational populations, particularly of the low-lying levels whose populations tend quickly to thermal equilibrium as  $n_H$  increases.

The rotational population of the ground state is controlled by neutral particle collisions and the intensities of the pure rotational transitions in  $v=0$  increase steadily with  $n_H$  towards the thermal equilibrium values.

To demonstrate the dependence of the emissivities on the ionization rate  $\zeta$  itself, we list in Tables 7a, 7b and 7c the emissivities per  $H_2$  molecules for ranges of  $\zeta$  at several values of  $n_H$  for a gas at temperatures of 500K, 1000K and 2000K. The corresponding fractional abundances  $n(H)$ ,  $n(H_2)$ ,  $n(H^+)$ ,  $n(e)$  and  $n(He^+)$  are shown in Fig. 2 as functions of  $(\zeta/n_H)$  for  $T = 2000K$ . The fractional abundances depend little on  $T$ .

For large  $\zeta$  and low densities and low temperatures, the intensities scale linearly with  $\zeta$ , but neutral particle collisions increase in relative importance as  $\zeta$  increases, as  $n_H$  increases and as  $T$  increases. The tendency for collisions to become dominant as  $\zeta$  decreases and as  $n_H$  increases is slowed by the conversion of H to  $H_2$  that also occurs. Neutral particle excitation is less important for the high vibrational levels and emission from them provides a more direct measure of the ionization flux. At high densities, collisional quenching is more rapid than radiative decay as a depopulation mechanism and the levels tend to a thermal distribution, indicated by LTE in the Tables.

Figs. 3a-d show the predicted emission spectra for an ionization rate given by  $(\zeta/n_H) = 10^{-17} \text{ cm}^3 \text{ s}^{-1}$  in a gas at 500K and with densities ranging from  $10 \text{ cm}^{-3}$  to  $10^7 \text{ cm}^{-3}$ . The theoretical spectra have been convolved with a Gaussian of FWHM  $0.01 \mu m$  representing the finite width of a spectrometer. Each pair of figures shows the results with and without the contribution of the photoelectron source.

At  $T=500K$ , neutral particle collisions are effective only in determining the relative populations of the low rotational states of the  $v=0$  vibrational level and the energetic photoelectrons populate the excited vibrational levels.

The lines from the  $v=1$  level are the strongest in the spectrum. They increase in intensity approximately as the density, though their relative strengths are modified as the rotational population in  $v=0$  changes. At high densities, the line intensities tend to a limit that is determined by the value of  $(\zeta/n_H)$ .

The ratio of the 2-1  $S(1)$  and 1-0  $S(1)$  line intensities is a widely used diagnostic probe. In Figs. 4a, b and c, we present the ratio for  $T=500K$ ,  $1000K$  and  $2000K$  and densities between  $10 \text{ cm}^{-3}$  and  $10^7 \text{ cm}^{-3}$  as a function of  $\zeta/n_H$  up to  $10^{-15} \text{ cm}^3 \text{ s}^{-1}$ . The variations with  $(\zeta/n_H)$  and  $n_H$  are complicated by the changes in the  $H/H_2$  ratio and the greater efficiency of collisions with  $H$  than with  $H_2$ . The increase in the ratio from one plateau to another in Figs. 4b and 4c for temperatures of  $1000K$  and  $200K$  respectively is a reflection of the conversion of  $H_2$  to  $H$ . The plateaux are not apparent in Fig. 4a because at  $500K$  and low  $(\zeta/n_H)$  neutral particle collisions have little effect. At all three temperatures, the ratios eventually increase with  $(\zeta/n_H)$ . The increases begin at the critical values of  $(\zeta/n_H)$ , where photoelectron pumping replaces neutral particle impact excitation as the major population mechanism. When the level populations are controlled by photoelectron pumping the ratio may also increase when the ionization fraction gets large enough that Coulomb heating competes with direct vibrational excitation of the  $v=1$  state. At  $500K$ , photoelectron pumping controls the populations of  $v=1$  and 2 for the entire range shown in Fig. 4 and for each density the change in ratio reflects the change in entry efficiencies as the ionization fraction changes. At  $1000K$  and low density the critical value for  $(v=2,J=3)$  as calculated from equation (3) is  $(\zeta/n_H)_{cr}=10^{-16} \text{ cm}^3 \text{ s}^{-1}$ . At this value the ratio increases as the level departs from the pure collisional value (see Fig. 4b). At the critical value of  $\zeta/n_H$  for  $(v=1,J=3)$  the ratio will flatten out to its limiting value. Our results are qualitatively similar to those of Maloney, Hollenbach and Tielens(1996). Maloney et al. carried out a less detailed calculation of the 2-1S(1) and 1-0S(1) line intensities for a range of values of  $\zeta$  but did take into account the variation of  $T$  with  $\zeta$ .

#### 4. Observations

Observational data on the 2-1  $S(1)/1-0S(1)$  ratio in external galaxies have been compiled by Mouri (1994) who has discussed the possible excitation mechanisms. For the Seyfert galaxy NGC 1275 the ratio is  $0.061 \pm 0.029$ , a value that occurs in a cold gas for a wide range of densities and X-ray fluxes. Alternatively, the value of 0.06 can be produced in a thermal gas heated to a temperature of  $1800K$ . A decisive test of the X-ray pumping mechanism would be provided by the measurement of the ratio of the intensities of lines from  $v \geq 3$  to lines from  $v=1$  or 2.

The work of AD was supported by the Division of Astronomical Science of the National Science Foundation under Grant AST95-31790. ST was partially supported by NSF Grant OSR-9353227, by NASA under grant NAGW-1561 and by the Università di Genova, Italy. SL was supported by NASA under grant NAGW-3147.

## REFERENCES

- Abgrall, H., Le Bourlot, J., Pineau des Forêts, G., Roueff, E., Flower, D.R., and Heck, L. 1992, *A&A*, 253, 525
- Audibert, M.M., Vilaseca R., Lukasik J., and Ducuing, J. 1976, *Chem. Phys. Lett.*, 37, 408
- Billing, G.D., and Kolesnick, R.E. 1993, *Chem. Phys. Lett.*, 215, 571
- Black, J.H., and van Dishoeck, E. 1987, *ApJ*, 322, 412
- Boothroyd, A.I., Keogh, W.J., Martin, P.G., and Peterson, M.R. 1991, *J.Chem.Phys.*, 95, 4343
- Cacciatore, M., Capitelli, M., and Billing, G.D. 1989, *Chem. Phys. Lett.*, 157, 305
- Cacciatore, M., and Billing, G.D. 1992, *J. Phys. Chem.*, 96, 217
- Danby, G., Flower, D.R., and Monteiro, T.S. 1987, *MNRAS*, 226, 739
- Draine, B.T., Roberge, W.G., and Dalgarno, A. 1983, *ApJ*, 264, 485
- Flower, D.R., and Wroe, R.A. 1997, *J. Phys. B* submitted
- Gerlich, D. 1990, *J. Chem. Phys.*, 92, 2377
- Gredel, R. and Dalgarno, A. 1995, *ApJ*, 446, 852
- Kolesnick, R.E., and Billing, G.D. 1993, *Chem. Phys.*, 170, 201
- Kreutz, T.G., Gelfand, J., Miles, R.B., and Rabitz, H. 1988, *Chem. Phys.*, 124, 359
- Lepp, S., Buch, V., and Dalgarno, A. 1995, *ApJS*, 98, 345
- Lepp, S., and Dalgarno, A. 1996, *A&A*, 306, L21
- Lepp, S., and McCray, R. 1983, *ApJ*, 269, 560
- Lepp, S., Tiné, S., and Dalgarno, A. 1997, *in preparation*
- Maloney, P.R., Hollenbach, D.J., and Tielens, A.G.G.M. 1996, *ApJ*, 466, 561
- Martin, P.G., and Mandy, M., 1995, *ApJ*, 455, L89
- Mouri, H. 1994, *ApJ*, 427, 777
- Schaefer, J., and Köhler, W.E. 1985, *Physica*, 129A, 469
- Sun, Y., and Dalgarno, A. 1994, *ApJ*, 427, 1053
- Sternberg, A., and Dalgarno, A. 1989, *ApJ*, 338, 197
- Teitelbaum, H. 1984, *Chem. Phys. Lett.*, 106, 69
- Varandas, A.J.C., Brown, F.B., Mead, C.A., Truhlar, D.G., and Blais, N.C. 1987, *J. Chem. Phys.*, 86, 6258

Table 1. Coefficients A, B and C for Arrhenius-type fits to H<sub>2</sub>-H<sub>2</sub> rate coefficients.\*

v	Q <sub>H<sub>2</sub></sub> (v,v-1;0,0)			Q <sub>H<sub>2</sub></sub> (1,0;v,v)			Q <sub>H<sub>2</sub></sub> (v,v-1;0,1)		
	A	B	C	A	B	C	A	B	C
1	-25.45	20.21	3.870	-25.33	0.00	3.78	-	-	-
2	-24.54	20.00	3.740	-25.02	0.00	3.70	-12.55	388.22	0.148
3	-23.68	20.00	3.640	-24.67	0.00	3.59	-14.13	223.45	0.433
4	-22.96	20.00	3.550	-24.42	0.00	3.51	-14.41	334.47	0.557
5	-21.62	20.00	3.260	-24.01	0.00	3.38	-14.40	467.55	0.593
6	-20.95	20.00	3.160	-24.01	0.00	3.84	-15.77	586.45	1.070
7	-18.85	20.00	2.590	-23.08	0.00	3.17	-18.57	614.46	2.000
8	-18.17	20.00	2.490	-21.52	0.00	2.65	-17.47	888.90	1.650
9	-17.35	20.00	2.300	-20.41	0.00	2.29	-16.20	1178.72	1.240
10	-15.47	20.00	1.730	-20.00	0.00	2.00	-20.24	1398.51	2.480
11	-14.64	20.00	1.530	-19.50	0.00	2.00	-21.29	1320.56	2.750
12	-13.35	20.00	1.150	-19.00	0.00	2.00	-22.16	1251.92	2.960
13	-12.87	20.00	1.040	-18.50	0.00	2.00	-23.22	1173.03	3.240
14	-12.18	20.00	0.857	-18.00	0.00	2.00	-24.11	1103.51	3.460

\*Numbers in italics are obtained by interpolation or extrapolation.

Table 2. Entry efficiencies  $\alpha_{J_i}(v, J)$  for fractional ionization  $x=10^{-6}$ .

$v$	$J-J_i$	$J_i=0$	$J_i=1$	$J_i=2$	$J_i=3$	$J_i=4$	$J_i=5$	$J_i=6$	$J_i=7$	$J_i=8$	$J_i=9$
0	-2	-	-	3.5(-3)	4.5(-3)	5.0(-3)	5.3(-3)	5.5(-3)	5.7(-3)	5.8(-3)	5.9(-3)
	0	1.2(-2)	1.9(-2)	1.7(-2)	1.7(-2)	1.7(-2)	1.7(-2)	1.7(-2)	1.7(-2)	1.7(-2)	1.7(-2)
	+2	1.8(-2)	1.0(-2)	9.0(-3)	8.4(-3)	8.0(-3)	7.8(-3)	7.6(-3)	7.5(-3)	7.4(-3)	7.3(-3)
1	-2	-	-	1.6	1.4	1.9	1.8	1.8	1.7	1.7	1.7
	0	2.4	2.4	2.1	2.1	3.1	3.1	3.1	3.1	3.1	3.1
	+2	2.4	2.4	4.7(-1)	7.0(-1)	1.2	1.2	1.3	1.3	1.4	1.4
2	-2	-	-	1.2(-1)	1.1(-1)	1.5(-1)	1.4(-1)	1.4(-1)	1.4(-1)	1.4(-1)	1.4(-1)
	0	1.9(-1)	1.9(-1)	1.7(-1)	1.7(-1)	2.5(-1)	2.5(-1)	2.5(-1)	2.5(-1)	2.5(-1)	2.5(-1)
	+2	1.9(-1)	1.8(-1)	4.0(-2)	5.7(-2)	9.4(-2)	1.0(-1)	1.0(-1)	1.1(-1)	1.1(-1)	1.1(-1)
3	-2	-	-	1.9(-3)	2.4(-3)	2.7(-3)	2.9(-3)	3.0(-3)	3.0(-3)	3.1(-3)	3.1(-3)
	0	6.9(-3)	1.1(-2)	9.5(-3)	9.3(-3)	9.3(-3)	9.3(-3)	9.3(-3)	9.2(-3)	9.2(-3)	9.2(-3)
	+2	9.4(-3)	5.6(-3)	4.8(-3)	4.5(-3)	4.3(-3)	4.1(-3)	4.1(-3)	4.0(-3)	3.9(-3)	3.9(-3)
4	-2	-	-	1.7(-3)	2.2(-3)	2.4(-3)	2.6(-3)	2.7(-3)	2.8(-3)	2.8(-3)	2.9(-3)
	0	6.4(-3)	9.8(-3)	8.8(-3)	8.6(-3)	8.6(-3)	8.6(-3)	8.6(-3)	8.5(-3)	8.5(-3)	8.5(-3)
	+2	8.5(-3)	5.1(-3)	4.4(-3)	4.1(-3)	3.9(-3)	3.8(-3)	3.7(-3)	3.6(-3)	3.6(-3)	3.5(-3)
5	-2	-	-	1.7(-3)	2.2(-3)	2.4(-3)	2.6(-3)	2.7(-3)	2.7(-3)	2.8(-3)	2.8(-3)
	0	6.2(-3)	9.6(-3)	8.6(-3)	8.4(-3)	8.4(-3)	8.4(-3)	8.3(-3)	8.3(-3)	8.3(-3)	8.3(-3)
	+2	8.4(-3)	5.1(-3)	4.3(-3)	4.0(-3)	3.8(-3)	3.7(-3)	3.6(-3)	3.6(-3)	3.5(-3)	3.5(-3)
6	-2	-	-	1.6(-3)	2.1(-3)	2.3(-3)	2.5(-3)	2.6(-3)	2.6(-3)	2.7(-3)	2.7(-3)
	0	5.8(-3)	9.1(-3)	8.1(-3)	8.0(-3)	7.9(-3)	7.9(-3)	7.9(-3)	7.9(-3)	7.9(-3)	7.9(-3)
	+2	8.2(-3)	4.9(-3)	4.2(-3)	3.9(-3)	3.7(-3)	3.6(-3)	3.5(-3)	3.5(-3)	3.4(-3)	3.4(-3)
7	-2	-	-	1.6(-3)	2.0(-3)	2.3(-3)	2.4(-3)	2.5(-3)	2.6(-3)	2.6(-3)	2.7(-3)
	0	5.3(-3)	8.5(-3)	7.6(-3)	7.4(-3)	7.4(-3)	7.3(-3)	7.3(-3)	7.3(-3)	7.3(-3)	7.3(-3)
	+2	7.9(-3)	4.8(-3)	4.1(-3)	3.8(-3)	3.6(-3)	3.5(-3)	3.4(-3)	3.4(-3)	3.3(-3)	3.3(-3)
8	-2	-	-	1.5(-3)	2.0(-3)	2.2(-3)	2.3(-3)	2.4(-3)	2.5(-3)	2.6(-3)	2.6(-3)
	0	4.8(-3)	7.9(-3)	7.0(-3)	6.9(-3)	6.9(-3)	6.8(-3)	6.8(-3)	6.8(-3)	6.8(-3)	6.8(-3)
	+2	7.7(-3)	4.6(-3)	4.0(-3)	3.7(-3)	3.5(-3)	3.4(-3)	3.3(-3)	3.3(-3)	3.2(-3)	3.2(-3)
9	-2	-	-	1.5(-3)	1.9(-3)	2.1(-3)	2.2(-3)	2.3(-3)	2.4(-3)	2.4(-3)	2.5(-3)
	0	4.4(-3)	7.3(-3)	6.4(-3)	6.3(-3)	6.3(-3)	6.2(-3)	6.2(-3)	6.2(-3)	6.2(-3)	6.2(-3)
	+2	7.3(-3)	4.4(-3)	3.8(-3)	3.5(-3)	3.3(-3)	3.2(-3)	3.2(-3)	3.1(-3)	3.1(-3)	3.0(-3)
10	-2	-	-	1.5(-3)	2.0(-3)	2.2(-3)	2.3(-3)	2.4(-3)	2.5(-3)	2.5(-3)	2.6(-3)
	0	4.3(-3)	7.4(-3)	6.5(-3)	6.3(-3)	6.3(-3)	6.3(-3)	6.3(-3)	6.3(-3)	6.3(-3)	6.3(-3)
	+2	7.7(-3)	4.6(-3)	3.9(-3)	3.7(-3)	3.5(-3)	3.4(-3)	3.3(-3)	3.3(-3)	3.2(-3)	3.2(-3)
11	-2	-	-	1.5(-3)	1.9(-3)	2.1(-3)	2.2(-3)	2.3(-3)	2.4(-3)	2.4(-3)	2.5(-3)
	0	4.0(-3)	6.9(-3)	6.1(-3)	6.0(-3)	5.9(-3)	5.9(-3)	5.9(-3)	5.9(-3)	5.9(-3)	5.9(-3)
	+2	7.4(-3)	4.4(-3)	3.8(-3)	3.5(-3)	3.4(-3)	3.3(-3)	3.2(-3)	3.1(-3)	3.1(-3)	3.1(-3)
12	-2	-	-	1.6(-3)	2.0(-3)	2.2(-3)	2.4(-3)	2.5(-3)	2.5(-3)	2.6(-3)	2.6(-3)
	0	4.1(-3)	7.2(-3)	6.3(-3)	6.2(-3)	6.1(-3)	6.1(-3)	6.1(-3)	6.1(-3)	6.1(-3)	6.1(-3)
	+2	7.8(-3)	4.7(-3)	4.0(-3)	3.7(-3)	3.6(-3)	3.4(-3)	3.4(-3)	3.3(-3)	3.3(-3)	3.2(-3)

Table 2—Continued

v	J-J <sub>i</sub>	J <sub>i</sub> =0	J <sub>i</sub> =1	J <sub>i</sub> =2	J <sub>i</sub> =3	J <sub>i</sub> =4	J <sub>i</sub> =5	J <sub>i</sub> =6	J <sub>i</sub> =7	J <sub>i</sub> =8	J <sub>i</sub> =9
13	-2	-	-	1.2(-3)	1.6(-3)	1.8(-3)	1.9(-3)	1.9(-3)	2.0(-3)	2.0(-3)	2.1(-3)
	0	3.2(-3)	5.6(-3)	4.9(-3)	4.8(-3)	4.8(-3)	4.8(-3)	4.8(-3)	4.7(-3)	4.7(-3)	4.7(-3)
	+2	6.2(-3)	3.7(-3)	3.2(-3)	2.9(-3)	2.8(-3)	2.7(-3)	2.7(-3)	2.6(-3)	2.6(-3)	2.6(-3)
14	-2	-	-	8.2(-4)	1.0(-3)	1.2(-3)	1.2(-3)	1.3(-3)	1.3(-3)	1.4(-3)	1.4(-3)
	0	2.1(-3)	3.7(-3)	3.2(-3)	3.2(-3)	3.1(-3)	3.1(-3)	3.1(-3)	3.1(-3)	3.1(-3)	3.1(-3)
	+2	4.1(-3)	2.5(-3)	2.1(-3)	1.9(-3)	1.9(-3)	1.8(-3)	1.8(-3)	1.7(-3)	1.7(-3)	1.7(-3)

Table 3. Entry efficiencies  $\alpha_{J_i}(v, J)$  for fractional ionization  $x=10^{-4}$ .

v	J-J <sub>i</sub>	J <sub>i</sub> =0	J <sub>i</sub> =1	J <sub>i</sub> =2	J <sub>i</sub> =3	J <sub>i</sub> =4	J <sub>i</sub> =5	J <sub>i</sub> =6	J <sub>i</sub> =7	J <sub>i</sub> =8	J <sub>i</sub> =9
0	-2	-	-	3.5(-3)	4.4(-3)	4.9(-3)	5.2(-3)	5.5(-3)	5.6(-3)	5.7(-3)	5.8(-3)
	0	1.2(-2)	1.9(-2)	1.7(-2)	1.7(-2)	1.6(-2)	1.6(-2)	1.6(-2)	1.6(-2)	1.6(-2)	1.6(-2)
	+2	1.7(-2)	1.0(-2)	8.9(-3)	8.2(-3)	7.9(-3)	7.6(-3)	7.5(-3)	7.3(-3)	7.2(-3)	7.2(-3)
1	-2	-	-	3.6(-1)	3.1(-1)	3.1(-1)	3.0(-1)	2.9(-1)	2.8(-1)	2.8(-1)	2.8(-1)
	0	4.8(-1)	4.8(-1)	4.7(-1)	4.7(-1)	5.0(-1)	5.0(-1)	5.0(-1)	5.0(-1)	5.0(-1)	5.0(-1)
	+2	4.9(-1)	4.8(-1)	1.1(-1)	1.6(-1)	1.9(-1)	2.0(-1)	2.1(-1)	2.2(-1)	2.2(-1)	2.2(-1)
2	-2	-	-	3.6(-2)	3.2(-2)	3.2(-2)	3.1(-2)	3.1(-2)	3.0(-2)	3.0(-2)	3.0(-2)
	0	5.2(-2)	5.6(-2)	5.4(-2)	5.3(-2)	5.7(-2)	5.7(-2)	5.7(-2)	5.7(-2)	5.7(-2)	5.7(-2)
	+2	5.5(-2)	5.1(-2)	1.5(-2)	1.9(-2)	2.2(-2)	2.3(-2)	2.4(-2)	2.5(-2)	2.5(-2)	2.5(-2)
3	-2	-	-	1.8(-3)	2.4(-3)	2.6(-3)	2.8(-3)	2.9(-3)	3.0(-3)	3.0(-3)	3.1(-3)
	0	6.8(-3)	1.0(-2)	9.4(-3)	9.2(-3)	9.2(-3)	9.1(-3)	9.1(-3)	9.1(-3)	9.1(-3)	9.1(-3)
	+2	9.2(-3)	5.5(-3)	4.7(-3)	4.4(-3)	4.2(-3)	4.1(-3)	4.0(-3)	3.9(-3)	3.9(-3)	3.8(-3)
4	-2	-	-	1.7(-3)	2.2(-3)	2.4(-3)	2.6(-3)	2.6(-3)	2.7(-3)	2.8(-3)	2.8(-3)
	0	6.3(-3)	9.6(-3)	8.7(-3)	8.5(-3)	8.5(-3)	8.4(-3)	8.4(-3)	8.4(-3)	8.4(-3)	8.4(-3)
	+2	8.4(-3)	5.0(-3)	4.3(-3)	4.0(-3)	3.8(-3)	3.7(-3)	3.6(-3)	3.6(-3)	3.5(-3)	3.5(-3)
5	-2	-	-	1.7(-3)	2.1(-3)	2.4(-3)	2.5(-3)	2.6(-3)	2.7(-3)	2.7(-3)	2.8(-3)
	0	6.1(-3)	9.4(-3)	8.5(-3)	8.3(-3)	8.3(-3)	8.2(-3)	8.2(-3)	8.2(-3)	8.2(-3)	8.2(-3)
	+2	8.3(-3)	5.0(-3)	4.3(-3)	3.9(-3)	3.8(-3)	3.7(-3)	3.6(-3)	3.5(-3)	3.5(-3)	3.4(-3)
6	-2	-	-	1.6(-3)	2.1(-3)	2.3(-3)	2.4(-3)	2.5(-3)	2.6(-3)	2.7(-3)	2.7(-3)
	0	5.7(-3)	8.9(-3)	8.0(-3)	7.8(-3)	7.8(-3)	7.8(-3)	7.8(-3)	7.7(-3)	7.7(-3)	7.7(-3)
	+2	8.1(-3)	4.8(-3)	4.1(-3)	3.8(-3)	3.7(-3)	3.6(-3)	3.5(-3)	3.4(-3)	3.4(-3)	3.3(-3)
7	-2	-	-	1.6(-3)	2.0(-3)	2.2(-3)	2.4(-3)	2.5(-3)	2.5(-3)	2.6(-3)	2.6(-3)
	0	5.2(-3)	8.3(-3)	7.4(-3)	7.3(-3)	7.2(-3)	7.2(-3)	7.2(-3)	7.2(-3)	7.2(-3)	7.2(-3)
	+2	7.8(-3)	4.7(-3)	4.0(-3)	3.7(-3)	3.6(-3)	3.4(-3)	3.4(-3)	3.3(-3)	3.3(-3)	3.2(-3)
8	-2	-	-	1.5(-3)	1.9(-3)	2.2(-3)	2.3(-3)	2.4(-3)	2.5(-3)	2.5(-3)	2.6(-3)
	0	4.8(-3)	7.8(-3)	6.9(-3)	6.8(-3)	6.8(-3)	6.7(-3)	6.7(-3)	6.7(-3)	6.7(-3)	6.7(-3)
	+2	7.6(-3)	4.6(-3)	3.9(-3)	3.6(-3)	3.5(-3)	3.4(-3)	3.3(-3)	3.2(-3)	3.2(-3)	3.2(-3)
9	-2	-	-	1.4(-3)	1.9(-3)	2.1(-3)	2.2(-3)	2.3(-3)	2.3(-3)	2.4(-3)	2.4(-3)
	0	4.3(-3)	7.2(-3)	6.3(-3)	6.2(-3)	6.2(-3)	6.1(-3)	6.1(-3)	6.1(-3)	6.1(-3)	6.1(-3)
	+2	7.2(-3)	4.3(-3)	3.7(-3)	3.4(-3)	3.3(-3)	3.2(-3)	3.1(-3)	3.0(-3)	3.0(-3)	3.0(-3)
10	-2	-	-	1.5(-3)	1.9(-3)	2.2(-3)	2.3(-3)	2.4(-3)	2.4(-3)	2.5(-3)	2.5(-3)
	0	4.2(-3)	7.3(-3)	6.4(-3)	6.2(-3)	6.2(-3)	6.2(-3)	6.2(-3)	6.2(-3)	6.2(-3)	6.1(-3)
	+2	7.5(-3)	4.5(-3)	3.9(-3)	3.6(-3)	3.4(-3)	3.3(-3)	3.3(-3)	3.2(-3)	3.2(-3)	3.1(-3)
11	-2	-	-	1.4(-3)	1.9(-3)	2.1(-3)	2.2(-3)	2.3(-3)	2.3(-3)	2.4(-3)	2.4(-3)
	0	3.9(-3)	6.8(-3)	6.0(-3)	5.9(-3)	5.8(-3)	5.8(-3)	5.8(-3)	5.8(-3)	5.8(-3)	5.8(-3)
	+2	7.2(-3)	4.4(-3)	3.7(-3)	3.4(-3)	3.3(-3)	3.2(-3)	3.1(-3)	3.1(-3)	3.0(-3)	3.0(-3)
12	-2	-	-	1.5(-3)	2.0(-3)	2.2(-3)	2.3(-3)	2.4(-3)	2.5(-3)	2.5(-3)	2.6(-3)
	0	4.0(-3)	7.1(-3)	6.2(-3)	6.1(-3)	6.0(-3)	6.0(-3)	6.0(-3)	6.0(-3)	6.0(-3)	6.0(-3)
	+2	7.7(-3)	4.6(-3)	3.9(-3)	3.7(-3)	3.5(-3)	3.4(-3)	3.3(-3)	3.3(-3)	3.2(-3)	3.2(-3)

Table 3—Continued

v	J-J <sub>i</sub>	J <sub>i</sub> =0	J <sub>i</sub> =1	J <sub>i</sub> =2	J <sub>i</sub> =3	J <sub>i</sub> =4	J <sub>i</sub> =5	J <sub>i</sub> =6	J <sub>i</sub> =7	J <sub>i</sub> =8	J <sub>i</sub> =9
13	-2	—	—	1.2(-3)	1.6(-3)	1.7(-3)	1.8(-3)	1.9(-3)	2.0(-3)	2.0(-3)	2.0(-3)
	0	3.1(-3)	5.5(-3)	4.9(-3)	4.7(-3)	4.7(-3)	4.7(-3)	4.7(-3)	4.7(-3)	4.7(-3)	4.7(-3)
	+2	6.1(-3)	3.6(-3)	3.1(-3)	2.9(-3)	2.8(-3)	2.7(-3)	2.6(-3)	2.6(-3)	2.5(-3)	2.5(-3)
14	-2	—	—	8.1(-4)	1.0(-3)	1.2(-3)	1.2(-3)	1.3(-3)	1.3(-3)	1.3(-3)	1.4(-3)
	0	2.0(-3)	3.6(-3)	3.2(-3)	3.1(-3)	3.1(-3)	3.1(-3)	3.1(-3)	3.1(-3)	3.0(-3)	3.0(-3)
	+2	4.0(-3)	2.4(-3)	2.1(-3)	1.9(-3)	1.8(-3)	1.8(-3)	1.7(-3)	1.7(-3)	1.7(-3)	1.7(-3)

Table 4. Entry efficiencies  $\alpha_{J_i}(v, J)$  for fractional ionization  $x=10^{-3}$ .

v	J-J <sub>i</sub>	J <sub>i</sub> =0	J <sub>i</sub> =1	J <sub>i</sub> =2	J <sub>i</sub> =3	J <sub>i</sub> =4	J <sub>i</sub> =5	J <sub>i</sub> =6	J <sub>i</sub> =7	J <sub>i</sub> =8	J <sub>i</sub> =9
0	-2	-	-	3.0(-3)	3.9(-3)	4.4(-3)	4.6(-3)	4.8(-3)	4.9(-3)	5.0(-3)	5.1(-3)
	0	1.1(-2)	1.7(-2)	1.5(-2)	1.5(-2)	1.5(-2)	1.5(-2)	1.5(-2)	1.5(-2)	1.4(-2)	1.4(-2)
	+2	1.5(-2)	9.1(-3)	7.8(-3)	7.2(-3)	6.9(-3)	6.7(-3)	6.6(-3)	6.5(-3)	6.4(-3)	6.3(-3)
1	-2	-	-	7.1(-2)	6.2(-2)	5.9(-2)	5.6(-2)	5.5(-2)	5.4(-2)	5.4(-2)	5.3(-2)
	0	9.7(-2)	1.0(-1)	9.9(-2)	9.9(-2)	9.9(-2)	9.9(-2)	9.9(-2)	9.9(-2)	9.9(-2)	9.9(-2)
	+2	9.9(-2)	9.5(-2)	2.5(-2)	3.4(-2)	3.8(-2)	4.1(-2)	4.2(-2)	4.3(-2)	4.4(-2)	4.4(-2)
2	-2	-	-	1.0(-2)	9.5(-3)	9.3(-3)	9.2(-3)	9.1(-3)	9.1(-3)	9.0(-3)	9.0(-3)
	0	1.7(-2)	2.1(-2)	2.0(-2)	2.0(-2)	2.0(-2)	2.0(-2)	2.0(-2)	2.0(-2)	1.9(-2)	1.9(-2)
	+2	2.0(-2)	1.6(-2)	6.8(-3)	7.7(-3)	8.0(-3)	8.2(-3)	8.3(-3)	8.4(-3)	8.4(-3)	8.4(-3)
3	-2	-	-	1.6(-3)	2.1(-3)	2.3(-3)	2.4(-3)	2.5(-3)	2.6(-3)	2.6(-3)	2.7(-3)
	0	6.0(-3)	9.2(-3)	8.3(-3)	8.1(-3)	8.1(-3)	8.1(-3)	8.1(-3)	8.1(-3)	8.0(-3)	8.0(-3)
	+2	8.0(-3)	4.8(-3)	4.1(-3)	3.8(-3)	3.7(-3)	3.6(-3)	3.5(-3)	3.4(-3)	3.4(-3)	3.3(-3)
4	-2	-	-	1.5(-3)	1.9(-3)	2.1(-3)	2.2(-3)	2.3(-3)	2.4(-3)	2.4(-3)	2.5(-3)
	0	5.6(-3)	8.5(-3)	7.7(-3)	7.5(-3)	7.5(-3)	7.5(-3)	7.5(-3)	7.5(-3)	7.4(-3)	7.4(-3)
	+2	7.3(-3)	4.4(-3)	3.8(-3)	3.5(-3)	3.3(-3)	3.2(-3)	3.2(-3)	3.1(-3)	3.1(-3)	3.0(-3)
5	-2	-	-	1.4(-3)	1.9(-3)	2.1(-3)	2.2(-3)	2.3(-3)	2.3(-3)	2.4(-3)	2.4(-3)
	0	5.4(-3)	8.3(-3)	7.5(-3)	7.3(-3)	7.3(-3)	7.3(-3)	7.3(-3)	7.3(-3)	7.3(-3)	7.2(-3)
	+2	7.2(-3)	4.3(-3)	3.7(-3)	3.4(-3)	3.3(-3)	3.2(-3)	3.1(-3)	3.1(-3)	3.0(-3)	3.0(-3)
6	-2	-	-	1.4(-3)	1.8(-3)	2.0(-3)	2.1(-3)	2.2(-3)	2.3(-3)	2.3(-3)	2.3(-3)
	0	5.0(-3)	7.8(-3)	7.0(-3)	6.9(-3)	6.9(-3)	6.9(-3)	6.8(-3)	6.8(-3)	6.8(-3)	6.8(-3)
	+2	7.0(-3)	4.2(-3)	3.6(-3)	3.3(-3)	3.2(-3)	3.1(-3)	3.0(-3)	3.0(-3)	2.9(-3)	2.9(-3)
7	-2	-	-	1.4(-3)	1.7(-3)	1.9(-3)	2.1(-3)	2.1(-3)	2.2(-3)	2.2(-3)	2.3(-3)
	0	4.6(-3)	7.3(-3)	6.5(-3)	6.4(-3)	6.4(-3)	6.3(-3)	6.3(-3)	6.3(-3)	6.3(-3)	6.3(-3)
	+2	6.8(-3)	4.1(-3)	3.5(-3)	3.2(-3)	3.1(-3)	3.0(-3)	2.9(-3)	2.9(-3)	2.8(-3)	2.8(-3)
8	-2	-	-	1.3(-3)	1.7(-3)	1.9(-3)	2.0(-3)	2.1(-3)	2.1(-3)	2.2(-3)	2.2(-3)
	0	4.2(-3)	6.8(-3)	6.0(-3)	5.9(-3)	5.9(-3)	5.9(-3)	5.8(-3)	5.8(-3)	5.8(-3)	5.8(-3)
	+2	6.6(-3)	3.9(-3)	3.4(-3)	3.1(-3)	3.0(-3)	2.9(-3)	2.8(-3)	2.8(-3)	2.7(-3)	2.7(-3)
9	-2	-	-	1.2(-3)	1.6(-3)	1.8(-3)	1.9(-3)	2.0(-3)	2.0(-3)	2.1(-3)	2.1(-3)
	0	3.8(-3)	6.3(-3)	5.5(-3)	5.4(-3)	5.4(-3)	5.4(-3)	5.4(-3)	5.3(-3)	5.3(-3)	5.3(-3)
	+2	6.2(-3)	3.7(-3)	3.2(-3)	3.0(-3)	2.8(-3)	2.7(-3)	2.6(-3)	2.6(-3)	2.6(-3)	2.6(-3)
10	-2	-	-	1.3(-3)	1.7(-3)	1.9(-3)	2.0(-3)	2.1(-3)	2.1(-3)	2.1(-3)	2.2(-3)
	0	3.7(-3)	6.3(-3)	5.5(-3)	5.4(-3)	5.4(-3)	5.4(-3)	5.3(-3)	5.3(-3)	5.3(-3)	5.3(-3)
	+2	6.5(-3)	3.9(-3)	3.3(-3)	3.1(-3)	3.0(-3)	2.9(-3)	2.8(-3)	2.8(-3)	2.7(-3)	2.7(-3)
11	-2	-	-	1.2(-3)	1.6(-3)	1.8(-3)	1.9(-3)	2.0(-3)	2.0(-3)	2.1(-3)	2.1(-3)
	0	3.4(-3)	5.9(-3)	5.2(-3)	5.1(-3)	5.1(-3)	5.0(-3)	5.0(-3)	5.0(-3)	5.0(-3)	5.0(-3)
	+2	6.3(-3)	3.8(-3)	3.2(-3)	3.0(-3)	2.9(-3)	2.8(-3)	2.7(-3)	2.7(-3)	2.6(-3)	2.6(-3)
12	-2	-	-	1.3(-3)	1.7(-3)	1.9(-3)	2.0(-3)	2.1(-3)	2.1(-3)	2.2(-3)	2.2(-3)
	0	3.5(-3)	6.1(-3)	5.4(-3)	5.2(-3)	5.2(-3)	5.2(-3)	5.2(-3)	5.2(-3)	5.2(-3)	5.2(-3)
	+2	6.6(-3)	4.0(-3)	3.4(-3)	3.2(-3)	3.0(-3)	2.9(-3)	2.9(-3)	2.8(-3)	2.7(-3)	2.7(-3)

Table 4—Continued

v	J-J <sub>i</sub>	J <sub>i</sub> =0	J <sub>i</sub> =1	J <sub>i</sub> =2	J <sub>i</sub> =3	J <sub>i</sub> =4	J <sub>i</sub> =5	J <sub>i</sub> =6	J <sub>i</sub> =7	J <sub>i</sub> =8	J <sub>i</sub> =9
13	-2	-	-	1.1(-3)	1.4(-3)	1.5(-3)	1.6(-3)	1.7(-3)	1.7(-3)	1.8(-3)	1.8(-3)
	0	2.7(-3)	4.9(-3)	4.3(-3)	4.1(-3)	4.1(-3)	4.1(-3)	4.1(-3)	4.1(-3)	4.1(-3)	4.1(-3)
	+2	5.3(-3)	3.2(-3)	2.7(-3)	2.5(-3)	2.4(-3)	2.3(-3)	2.3(-3)	2.2(-3)	2.2(-3)	2.2(-3)
14	-2	-	-	7.0(-4)	9.1(-4)	1.0(-3)	1.1(-3)	1.1(-3)	1.1(-3)	1.2(-3)	1.2(-3)
	0	1.8(-3)	3.2(-3)	2.8(-3)	2.7(-3)	2.7(-3)	2.7(-3)	2.7(-3)	2.7(-3)	2.7(-3)	2.7(-3)
	+2	3.5(-3)	2.1(-3)	1.8(-3)	1.7(-3)	1.6(-3)	1.6(-3)	1.5(-3)	1.5(-3)	1.5(-3)	1.5(-3)

Table 5. Entry efficiencies  $\alpha_{J_i}(v, J)$  for fractional ionization  $x=10^{-2}$ .

$v$	$J-J_i$	$J_i=0$	$J_i=1$	$J_i=2$	$J_i=3$	$J_i=4$	$J_i=5$	$J_i=6$	$J_i=7$	$J_i=8$	$J_i=9$
0	-2	-	-	1.8(-3)	2.3(-3)	2.6(-3)	2.7(-3)	2.8(-3)	2.9(-3)	3.0(-3)	3.0(-3)
	0	6.1(-3)	9.7(-3)	8.7(-3)	8.5(-3)	8.4(-3)	8.4(-3)	8.4(-3)	8.4(-3)	8.4(-3)	8.4(-3)
	+2	9.0(-3)	5.4(-3)	4.6(-3)	4.3(-3)	4.1(-3)	4.0(-3)	3.9(-3)	3.8(-3)	3.8(-3)	3.7(-3)
1	-2	-	-	1.5(-2)	1.3(-2)	1.2(-2)	1.2(-2)	1.2(-2)	1.2(-2)	1.2(-2)	1.2(-2)
	0	2.1(-2)	2.3(-2)	2.3(-2)	2.3(-2)	2.3(-2)	2.3(-2)	2.3(-2)	2.3(-2)	2.3(-2)	2.3(-2)
	+2	2.3(-2)	2.1(-2)	6.8(-3)	8.5(-3)	9.2(-3)	9.5(-3)	9.7(-3)	9.9(-3)	1.0(-2)	1.0(-2)
2	-2	-	-	3.2(-3)	3.2(-3)	3.2(-3)	3.2(-3)	3.2(-3)	3.2(-3)	3.2(-3)	3.2(-3)
	0	6.4(-3)	8.3(-3)	7.8(-3)	7.7(-3)	7.6(-3)	7.6(-3)	7.6(-3)	7.6(-3)	7.6(-3)	7.6(-3)
	+2	7.8(-3)	5.8(-3)	3.2(-3)	3.3(-3)	3.3(-3)	3.3(-3)	3.3(-3)	3.3(-3)	3.3(-3)	3.3(-3)
3	-2	-	-	9.5(-4)	1.2(-3)	1.4(-3)	1.4(-3)	1.5(-3)	1.5(-3)	1.6(-3)	1.6(-3)
	0	3.4(-3)	5.3(-3)	4.7(-3)	4.7(-3)	4.6(-3)	4.6(-3)	4.6(-3)	4.6(-3)	4.6(-3)	4.6(-3)
	+2	4.7(-3)	2.8(-3)	2.4(-3)	2.3(-3)	2.2(-3)	2.1(-3)	2.0(-3)	2.0(-3)	2.0(-3)	2.0(-3)
4	-2	-	-	8.6(-4)	1.1(-3)	1.2(-3)	1.3(-3)	1.4(-3)	1.4(-3)	1.4(-3)	1.4(-3)
	0	3.2(-3)	4.9(-3)	4.4(-3)	4.3(-3)	4.3(-3)	4.3(-3)	4.3(-3)	4.3(-3)	4.3(-3)	4.3(-3)
	+2	4.3(-3)	2.6(-3)	2.2(-3)	2.1(-3)	2.0(-3)	1.9(-3)	1.9(-3)	1.8(-3)	1.8(-3)	1.8(-3)
5	-2	-	-	8.5(-4)	1.1(-3)	1.2(-3)	1.3(-3)	1.3(-3)	1.4(-3)	1.4(-3)	1.4(-3)
	0	3.1(-3)	4.8(-3)	4.3(-3)	4.2(-3)	4.2(-3)	4.2(-3)	4.1(-3)	4.1(-3)	4.1(-3)	4.1(-3)
	+2	4.3(-3)	2.6(-3)	2.2(-3)	2.0(-3)	1.9(-3)	1.9(-3)	1.8(-3)	1.8(-3)	1.8(-3)	1.8(-3)
6	-2	-	-	8.2(-4)	1.1(-3)	1.2(-3)	1.2(-3)	1.3(-3)	1.3(-3)	1.4(-3)	1.4(-3)
	0	2.9(-3)	4.5(-3)	4.0(-3)	4.0(-3)	3.9(-3)	3.9(-3)	3.9(-3)	3.9(-3)	3.9(-3)	3.9(-3)
	+2	4.1(-3)	2.5(-3)	2.1(-3)	2.0(-3)	1.9(-3)	1.8(-3)	1.8(-3)	1.7(-3)	1.7(-3)	1.7(-3)
7	-2	-	-	8.0(-4)	1.0(-3)	1.2(-3)	1.2(-3)	1.3(-3)	1.3(-3)	1.3(-3)	1.3(-3)
	0	2.6(-3)	4.2(-3)	3.8(-3)	3.7(-3)	3.7(-3)	3.7(-3)	3.7(-3)	3.6(-3)	3.6(-3)	3.6(-3)
	+2	4.0(-3)	2.4(-3)	2.1(-3)	1.9(-3)	1.8(-3)	1.8(-3)	1.7(-3)	1.7(-3)	1.7(-3)	1.7(-3)
8	-2	-	-	7.8(-4)	1.0(-3)	1.1(-3)	1.2(-3)	1.2(-3)	1.3(-3)	1.3(-3)	1.3(-3)
	0	2.4(-3)	4.0(-3)	3.5(-3)	3.4(-3)	3.4(-3)	3.4(-3)	3.4(-3)	3.4(-3)	3.4(-3)	3.4(-3)
	+2	3.9(-3)	2.3(-3)	2.0(-3)	1.9(-3)	1.8(-3)	1.7(-3)	1.7(-3)	1.6(-3)	1.6(-3)	1.6(-3)
9	-2	-	-	7.4(-4)	9.6(-4)	1.1(-3)	1.1(-3)	1.2(-3)	1.2(-3)	1.2(-3)	1.2(-3)
	0	2.2(-3)	3.7(-3)	3.3(-3)	3.2(-3)	3.2(-3)	3.1(-3)	3.1(-3)	3.1(-3)	3.1(-3)	3.1(-3)
	+2	3.7(-3)	2.2(-3)	1.9(-3)	1.8(-3)	1.7(-3)	1.6(-3)	1.6(-3)	1.6(-3)	1.5(-3)	1.5(-3)
10	-2	-	-	7.8(-4)	1.0(-3)	1.1(-3)	1.2(-3)	1.2(-3)	1.3(-3)	1.3(-3)	1.3(-3)
	0	2.2(-3)	3.7(-3)	3.3(-3)	3.2(-3)	3.2(-3)	3.2(-3)	3.2(-3)	3.2(-3)	3.2(-3)	3.2(-3)
	+2	3.9(-3)	2.3(-3)	2.0(-3)	1.9(-3)	1.8(-3)	1.7(-3)	1.7(-3)	1.6(-3)	1.6(-3)	1.6(-3)
11	-2	-	-	7.5(-4)	9.7(-4)	1.1(-3)	1.1(-3)	1.2(-3)	1.2(-3)	1.2(-3)	1.3(-3)
	0	2.0(-3)	3.5(-3)	3.1(-3)	3.0(-3)	3.0(-3)	3.0(-3)	3.0(-3)	3.0(-3)	3.0(-3)	3.0(-3)
	+2	3.8(-3)	2.3(-3)	1.9(-3)	1.8(-3)	1.7(-3)	1.7(-3)	1.6(-3)	1.6(-3)	1.6(-3)	1.6(-3)
12	-2	-	-	8.0(-4)	1.0(-3)	1.1(-3)	1.2(-3)	1.2(-3)	1.3(-3)	1.3(-3)	1.3(-3)
	0	2.1(-3)	3.7(-3)	3.2(-3)	3.1(-3)	3.1(-3)	3.1(-3)	3.1(-3)	3.1(-3)	3.1(-3)	3.1(-3)
	+2	4.0(-3)	2.4(-3)	2.1(-3)	1.9(-3)	1.8(-3)	1.8(-3)	1.7(-3)	1.7(-3)	1.7(-3)	1.6(-3)

Table 5—Continued

v	J-J <sub>i</sub>	J <sub>i</sub> =0	J <sub>i</sub> =1	J <sub>i</sub> =2	J <sub>i</sub> =3	J <sub>i</sub> =4	J <sub>i</sub> =5	J <sub>i</sub> =6	J <sub>i</sub> =7	J <sub>i</sub> =8	J <sub>i</sub> =9
13	-2	—	—	6.4(-4)	8.2(-4)	9.1(-4)	9.7(-4)	1.0(-3)	1.0(-3)	1.0(-3)	1.1(-3)
	0	1.6(-3)	2.9(-3)	2.6(-3)	2.5(-3)	2.5(-3)	2.5(-3)	2.5(-3)	2.5(-3)	2.5(-3)	2.5(-3)
	+2	3.2(-3)	1.9(-3)	1.6(-3)	1.5(-3)	1.4(-3)	1.4(-3)	1.4(-3)	1.4(-3)	1.3(-3)	1.3(-3)
14	-2	—	—	4.3(-4)	5.5(-4)	6.1(-4)	6.5(-4)	6.7(-4)	6.9(-4)	7.0(-4)	7.1(-4)
	0	1.1(-3)	1.9(-3)	1.7(-3)	1.6(-3)	1.6(-3)	1.6(-3)	1.6(-3)	1.6(-3)	1.6(-3)	1.6(-3)
	+2	2.1(-3)	1.3(-3)	1.1(-3)	1.0(-3)	9.7(-4)	9.4(-4)	9.2(-4)	9.0(-4)	8.9(-4)	8.8(-4)

**Table 6a.** Emissivities  $\epsilon$  (erg s $^{-1}$ ) of selected H<sub>2</sub> lines as a function of n<sub>H</sub> (cm $^{-3}$ ) at T=500K,  
 $\zeta/n_H = 10^{-17}$  cm $^3$  s $^{-1}$

Line	$\lambda(\mu\text{m})$	n <sub>H</sub> =10 <sup>1</sup>	n <sub>H</sub> =10 <sup>3</sup>	n <sub>H</sub> =10 <sup>5</sup>	n <sub>H</sub> =10 <sup>7</sup>	LTE
0-0S(7)	5.508	9.70(-32)	2.42(-29)	1.36(-26)	2.47(-25)	1.87(-25)
1-0S(0)	2.222	1.12(-29)	1.12(-27)	1.11(-25)	1.67(-24)	2.15(-25)
1-0S(1)	2.121	4.60(-29)	4.56(-27)	3.81(-25)	4.00(-24)	4.96(-25)
1-0S(2)	2.033	2.46(-30)	3.72(-28)	4.75(-26)	6.92(-25)	7.15(-25)
2-1S(1)	2.247	3.39(-30)	3.27(-28)	1.90(-26)	6.19(-26)	9.12(-30)
5-3O(3)	1.613	8.30(-31)	6.71(-29)	1.03(-27)	1.41(-27)	5.90(-42)
6-4Q(1)	1.601	7.48(-31)	5.94(-29)	7.77(-28)	9.86(-28)	1.28(-45)

**Table 6b.** Emissivities  $\epsilon$  (erg s $^{-1}$ ) of selected H $_2$  lines as a function of n $_H$  (cm $^{-3}$ ) at T=1000K,  
 $\zeta/n_H = 10^{-17}$  cm $^3$  s $^{-1}$

Line	$\lambda(\mu\text{m})$	n $_H = 10^1$	n $_H = 10^3$	n $_H = 10^5$	n $_H = 10^7$	LTE
0-0S(7)	5.508	3.94(-27)	6.95(-25)	7.14(-23)	1.27(-22)	1.28(-22)
1-0S(0)	2.222	2.51(-27)	2.96(-25)	2.28(-23)	6.96(-23)	7.09(-23)
1-0S(1)	2.121	6.81(-27)	9.05(-25)	8.25(-23)	2.60(-22)	2.65(-22)
1-0S(2)	2.033	1.51(-27)	1.88(-25)	2.10(-23)	7.05(-23)	7.19(-23)
2-1S(1)	2.247	2.14(-29)	3.50(-27)	4.07(-25)	1.31(-24)	1.32(-24)
5-3O(3)	1.613	7.93(-31)	5.34(-29)	4.33(-28)	5.08(-28)	1.24(-30)
6-4Q(1)	1.601	7.12(-31)	4.66(-29)	3.43(-28)	3.88(-28)	2.05(-32)

**Table 6c.** Emissivities  $\epsilon$  (erg s $^{-1}$ ) of selected H $_2$  lines as a function of n $_H$  (cm $^{-3}$ ) at T=2000K,  
 $\zeta/n_H = 10^{-17}$  cm $^3$  s $^{-1}$

Line	$\lambda(\mu\text{m})$	n $_H=10^1$	n $_H=10^3$	n $_H=10^5$	n $_H=10^7$	LTE
0-0S(7)	5.508	1.11(-24)	1.90(-22)	2.03(-21)	2.21(-21)	2.21(-21)
1-0S(0)	2.222	1.63(-25)	1.81(-23)	6.08(-22)	8.50(-22)	8.53(-22)
1-0S(1)	2.121	6.26(-25)	7.63(-23)	2.86(-21)	4.03(-21)	4.05(-21)
1-0S(2)	2.033	2.05(-25)	2.60(-23)	1.06(-21)	1.50(-21)	1.51(-21)
2-1S(1)	2.247	2.08(-26)	3.29(-24)	2.11(-22)	3.30(-22)	3.32(-22)
5-3O(3)	1.613	3.46(-30)	7.72(-28)	2.03(-25)	3.75(-25)	3.77(-25)
6-4Q(1)	1.601	8.19(-31)	9.04(-29)	2.80(-26)	5.41(-26)	5.44(-26)

Table 7a. Emissivities  $\epsilon$  (erg s $^{-1}$ ) of selected H<sub>2</sub> lines as a function of  $\zeta$  (s $^{-1}$ ) at T=500K

$n_H = 10 \text{ cm}^{-3}$	Line	$\lambda(\mu\text{m})$	$\zeta = 10^{-17} \text{ s}^{-1}$	$\zeta = 10^{-16} \text{ s}^{-1}$	$\zeta = 10^{-15} \text{ s}^{-1}$	$\zeta = 10^{-14} \text{ s}^{-1}$
	0-0S(7)	5.508	7.53(-33)	9.70(-32)	1.37(-29)	7.55(-29)
	1-0S(0)	2.222	1.68(-30)	1.12(-29)	1.11(-29)	4.00(-29)
	1-0S(1)	2.121	7.36(-30)	4.60(-29)	3.79(-29)	1.45(-28)
	1-0S(2)	2.033	3.80(-31)	2.46(-30)	5.19(-30)	2.79(-29)
	2-1S(1)	2.247	4.53(-31)	3.39(-30)	9.17(-30)	5.29(-29)
	5-3O(3)	1.613	8.40(-32)	8.30(-31)	6.18(-30)	3.82(-29)
	6-4Q(1)	1.601	7.57(-32)	7.48(-31)	5.55(-30)	3.43(-29)
$n_H = 10^3 \text{ cm}^{-3}$	Line	$\lambda(\mu\text{m})$	$\zeta = 10^{-17} \text{ s}^{-1}$	$\zeta = 10^{-16} \text{ s}^{-1}$	$\zeta = 10^{-14} \text{ s}^{-1}$	$\zeta = 10^{-12} \text{ s}^{-1}$
	0-0S(7)	5.508	1.45(-32)	1.44(-30)	2.42(-29)	1.63(-26)
	1-0S(0)	2.222	2.00(-30)	1.72(-28)	1.12(-27)	3.65(-27)
	1-0S(1)	2.121	8.26(-30)	7.17(-28)	4.56(-27)	1.41(-26)
	1-0S(2)	2.033	6.51(-31)	5.66(-29)	3.72(-28)	2.94(-27)
	2-1S(1)	2.247	4.62(-31)	4.38(-29)	3.27(-28)	4.87(-27)
	5-3O(3)	1.613	7.41(-32)	7.31(-30)	6.71(-29)	2.86(-27)
	6-4Q(1)	1.601	6.60(-32)	6.51(-30)	5.94(-29)	2.51(-27)
$n_H = 10^5 \text{ cm}^{-3}$	Line	$\lambda(\mu\text{m})$	$\zeta = 10^{-17} \text{ s}^{-1}$	$\zeta = 10^{-16} \text{ s}^{-1}$	$\zeta = 10^{-12} \text{ s}^{-1}$	$\zeta = 10^{-10} \text{ s}^{-1}$
	0-0S(7)	5.508	2.58(-28)	3.65(-28)	1.36(-26)	2.02(-25)
	1-0S(0)	2.222	1.31(-29)	2.01(-27)	1.11(-25)	2.52(-25)
	1-0S(1)	2.121	3.22(-29)	7.19(-27)	3.81(-25)	9.06(-25)
	1-0S(2)	2.033	4.28(-30)	8.70(-28)	4.75(-26)	2.07(-25)
	2-1S(1)	2.247	4.36(-31)	4.23(-28)	1.90(-26)	1.68(-25)
	5-3O(3)	1.613	7.11(-32)	6.40(-29)	1.03(-27)	2.80(-26)
	6-4Q(1)	1.601	6.27(-32)	5.60(-29)	7.77(-28)	2.05(-26)
$n_H = 10^7 \text{ cm}^{-3}$	Line	$\lambda(\mu\text{m})$	$\zeta = 10^{-17} \text{ s}^{-1}$	$\zeta = 10^{-16} \text{ s}^{-1}$	$\zeta = 10^{-11} \text{ s}^{-1}$	$\zeta = 10^{-8} \text{ s}^{-1}$
	0-0S(7)	5.508	8.72(-26)	8.72(-26)	1.51(-25)	2.15(-25)
	1-0S(0)	2.222	1.08(-27)	3.41(-27)	1.09(-24)	2.38(-24)
	1-0S(1)	2.121	2.22(-27)	7.74(-27)	2.47(-24)	6.36(-24)
	1-0S(2)	2.033	3.64(-28)	1.16(-27)	3.93(-25)	1.50(-24)
	2-1S(1)	2.247	2.71(-31)	2.62(-28)	4.74(-26)	4.17(-25)
	5-3O(3)	1.613	7.30(-32)	6.95(-29)	1.16(-27)	3.35(-26)
	6-4Q(1)	1.601	6.96(-32)	6.62(-29)	8.15(-28)	2.34(-26)

Table 7b. Emissivities  $\epsilon$  (erg s $^{-1}$ ) of selected H $_2$  lines as a function of  $\zeta$  (s $^{-1}$ ) at T=1000K

$n_H = 10 \text{ cm}^{-3}$	Line	$\lambda(\mu\text{m})$	$\zeta = 10^{-17} \text{ s}^{-1}$	$\zeta = 10^{-16} \text{ s}^{-1}$	$\zeta = 10^{-15} \text{ s}^{-1}$	$\zeta = 10^{-14} \text{ s}^{-1}$
	0-0S(7)	5.508	4.78(-28)	3.94(-27)	2.65(-26)	1.02(-25)
	1-0S(0)	2.222	3.16(-28)	2.51(-27)	5.08(-27)	5.44(-27)
	1-0S(1)	2.121	8.56(-28)	6.81(-27)	1.38(-26)	1.53(-26)
	1-0S(2)	2.033	1.89(-28)	1.51(-27)	3.04(-27)	3.25(-27)
	2-1S(1)	2.247	2.66(-30)	2.14(-29)	4.65(-29)	9.54(-29)
	5-3O(3)	1.613	8.00(-32)	7.93(-31)	5.69(-30)	3.42(-29)
	6-4Q(1)	1.601	7.19(-32)	7.12(-31)	5.09(-30)	3.04(-29)
$n_H = 10^3 \text{ cm}^{-3}$	Line	$\lambda(\mu\text{m})$	$\zeta = 10^{-17} \text{ s}^{-1}$	$\zeta = 10^{-16} \text{ s}^{-1}$	$\zeta = 10^{-15} \text{ s}^{-1}$	$\zeta = 10^{-14} \text{ s}^{-1}$
	0-0S(7)	5.508	9.62(-28)	7.78(-26)	6.95(-25)	1.59(-23)
	1-0S(0)	2.222	9.89(-28)	3.68(-26)	2.96(-25)	6.50(-25)
	1-0S(1)	2.121	3.03(-27)	1.11(-25)	9.05(-25)	2.08(-24)
	1-0S(2)	2.033	6.37(-28)	2.28(-26)	1.88(-25)	4.52(-25)
	2-1S(1)	2.247	5.34(-30)	4.09(-28)	3.50(-27)	1.35(-26)
	5-3O(3)	1.613	6.44(-32)	6.28(-30)	5.34(-29)	2.03(-27)
	6-4Q(1)	1.601	5.65(-32)	5.50(-30)	4.66(-29)	1.76(-27)
$n_H = 10^5 \text{ cm}^{-3}$	Line	$\lambda(\mu\text{m})$	$\zeta = 10^{-17} \text{ s}^{-1}$	$\zeta = 10^{-16} \text{ s}^{-1}$	$\zeta = 10^{-15} \text{ s}^{-1}$	$\zeta = 10^{-14} \text{ s}^{-1}$
	0-0S(7)	5.508	4.38(-24)	6.06(-24)	7.14(-23)	1.20(-22)
	1-0S(0)	2.222	6.46(-26)	4.65(-25)	2.28(-23)	3.55(-23)
	1-0S(1)	2.121	2.34(-25)	1.61(-24)	8.25(-23)	1.30(-22)
	1-0S(2)	2.033	6.67(-26)	3.84(-25)	2.10(-23)	3.40(-23)
	2-1S(1)	2.247	1.77(-28)	7.00(-27)	4.07(-25)	7.21(-25)
	5-3O(3)	1.613	5.35(-32)	4.57(-29)	4.33(-28)	1.08(-26)
	6-4Q(1)	1.601	4.71(-32)	4.01(-29)	3.43(-28)	8.40(-27)
$n_H = 10^7 \text{ cm}^{-3}$	Line	$\lambda(\mu\text{m})$	$\zeta = 10^{-17} \text{ s}^{-1}$	$\zeta = 10^{-16} \text{ s}^{-1}$	$\zeta = 10^{-15} \text{ s}^{-1}$	$\zeta = 10^{-14} \text{ s}^{-1}$
	0-0S(7)	5.508	1.11(-22)	1.11(-22)	1.22(-22)	1.28(-22)
	1-0S(0)	2.222	6.07(-24)	6.41(-24)	6.10(-23)	7.04(-23)
	1-0S(1)	2.121	2.11(-23)	2.25(-23)	2.28(-22)	2.63(-22)
	1-0S(2)	2.033	6.17(-24)	6.51(-24)	6.16(-23)	7.14(-23)
	2-1S(1)	2.247	2.35(-26)	2.92(-26)	1.14(-24)	1.42(-24)
	5-3O(3)	1.613	2.87(-32)	2.42(-29)	4.28(-28)	1.18(-26)
	6-4Q(1)	1.601	1.51(-32)	1.47(-29)	3.38(-28)	8.98(-27)

Table 7c. Emissivities  $\epsilon$  (erg s $^{-1}$ ) of selected H $_2$  lines as a function of  $\zeta$  (s $^{-1}$ ) at T=2000K

$n_H = 10 \text{ cm}^{-3}$	Line	$\lambda(\mu\text{m})$	$\zeta = 10^{-17} \text{ s}^{-1}$	$\zeta = 10^{-16} \text{ s}^{-1}$	$\zeta = 10^{-15} \text{ s}^{-1}$	$\zeta = 10^{-14} \text{ s}^{-1}$
	0-0S(7)	5.508	1.29(-25)	1.11(-24)	3.15(-24)	6.20(-24)
	1-0S(0)	2.222	2.16(-26)	1.63(-25)	3.31(-25)	3.36(-25)
	1-0S(1)	2.121	8.16(-26)	6.26(-25)	1.28(-24)	1.32(-24)
	1-0S(2)	2.033	2.62(-26)	2.05(-25)	4.17(-25)	4.26(-25)
	2-1S(1)	2.247	2.52(-27)	2.08(-26)	4.38(-26)	4.59(-26)
	5-3O(3)	1.613	3.83(-31)	3.46(-30)	1.08(-29)	3.49(-29)
	6-4Q(1)	1.601	8.97(-32)	8.19(-31)	4.53(-30)	2.51(-29)
$n_H = 10^3 \text{ cm}^{-3}$	Line	$\lambda(\mu\text{m})$	$\zeta = 10^{-17} \text{ s}^{-1}$	$\zeta = 10^{-16} \text{ s}^{-1}$	$\zeta = 10^{-15} \text{ s}^{-1}$	$\zeta = 10^{-14} \text{ s}^{-1}$
	0-0S(7)	5.508	7.36(-25)	2.10(-23)	1.90(-22)	6.96(-22)
	1-0S(0)	2.222	1.90(-25)	2.31(-24)	1.81(-23)	3.78(-23)
	1-0S(1)	2.121	7.95(-25)	9.48(-24)	7.63(-23)	1.64(-22)
	1-0S(2)	2.033	2.51(-25)	3.14(-24)	2.60(-23)	5.71(-23)
	2-1S(1)	2.247	1.12(-26)	3.58(-25)	3.29(-24)	7.64(-24)
	5-3O(3)	1.613	6.44(-31)	6.38(-29)	7.72(-28)	3.55(-27)
	6-4Q(1)	1.601	8.28(-32)	8.40(-30)	9.04(-29)	1.28(-27)
$n_H = 10^5 \text{ cm}^{-3}$	Line	$\lambda(\mu\text{m})$	$\zeta = 10^{-17} \text{ s}^{-1}$	$\zeta = 10^{-16} \text{ s}^{-1}$	$\zeta = 10^{-15} \text{ s}^{-1}$	$\zeta = 10^{-14} \text{ s}^{-1}$
	0-0S(7)	5.508	7.18(-22)	8.67(-22)	2.03(-21)	2.17(-21)
	1-0S(0)	2.222	1.33(-23)	3.54(-23)	6.08(-22)	7.14(-22)
	1-0S(1)	2.121	6.09(-23)	1.62(-22)	2.86(-21)	3.38(-21)
	1-0S(2)	2.033	2.41(-23)	6.11(-23)	1.06(-21)	1.25(-21)
	2-1S(1)	2.247	7.65(-25)	5.70(-24)	2.11(-22)	2.61(-22)
	5-3O(3)	1.613	1.71(-29)	1.64(-27)	2.03(-25)	2.77(-25)
	6-4Q(1)	1.601	1.01(-30)	1.68(-28)	2.80(-26)	4.17(-26)
$n_H = 10^7 \text{ cm}^{-3}$	Line	$\lambda(\mu\text{m})$	$\zeta = 10^{-17} \text{ s}^{-1}$	$\zeta = 10^{-16} \text{ s}^{-1}$	$\zeta = 10^{-15} \text{ s}^{-1}$	$\zeta = 10^{-14} \text{ s}^{-1}$
	0-0S(7)	5.508	2.22(-21)	2.22(-21)	2.20(-21)	2.21(-21)
	1-0S(0)	2.222	5.27(-22)	5.31(-22)	5.27(-22)	8.52(-22)
	1-0S(1)	2.121	2.47(-21)	2.49(-21)	3.93(-21)	4.04(-21)
	1-0S(2)	2.033	9.34(-22)	9.40(-22)	1.46(-21)	1.51(-21)
	2-1S(1)	2.247	1.39(-22)	1.42(-22)	3.18(-22)	3.31(-22)
	5-3O(3)	1.613	1.16(-25)	1.19(-25)	3.57(-25)	3.81(-25)
	6-4Q(1)	1.601	1.62(-26)	1.65(-26)	5.13(-26)	5.77(-26)

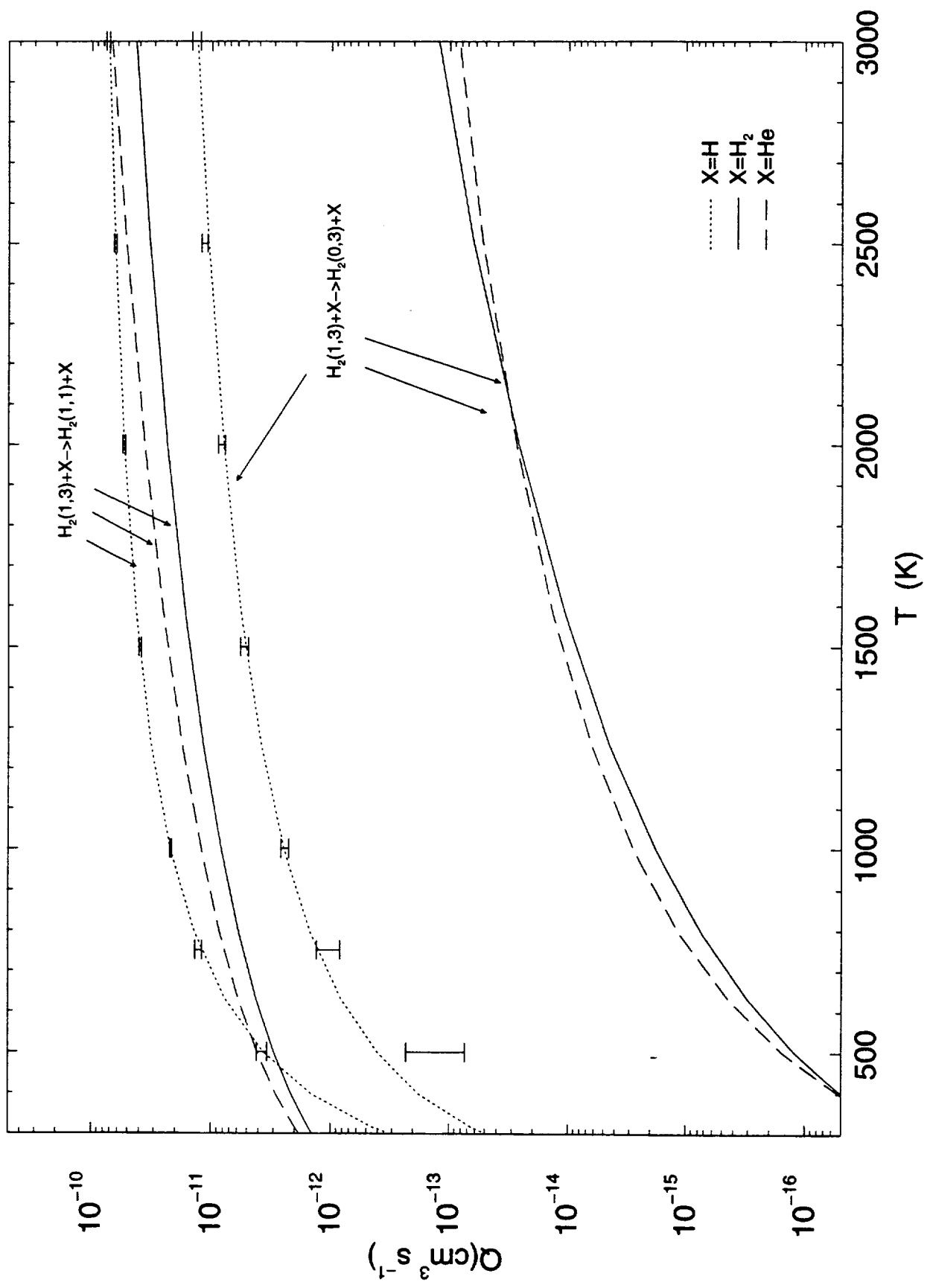
Fig. 1.— Comparison of rate coefficients for collisions of H<sub>2</sub> with H, H<sub>2</sub> and He.

Fig. 2.— Fractional abundances as a function of  $\zeta/n_H$  in a gas at T=2000K.

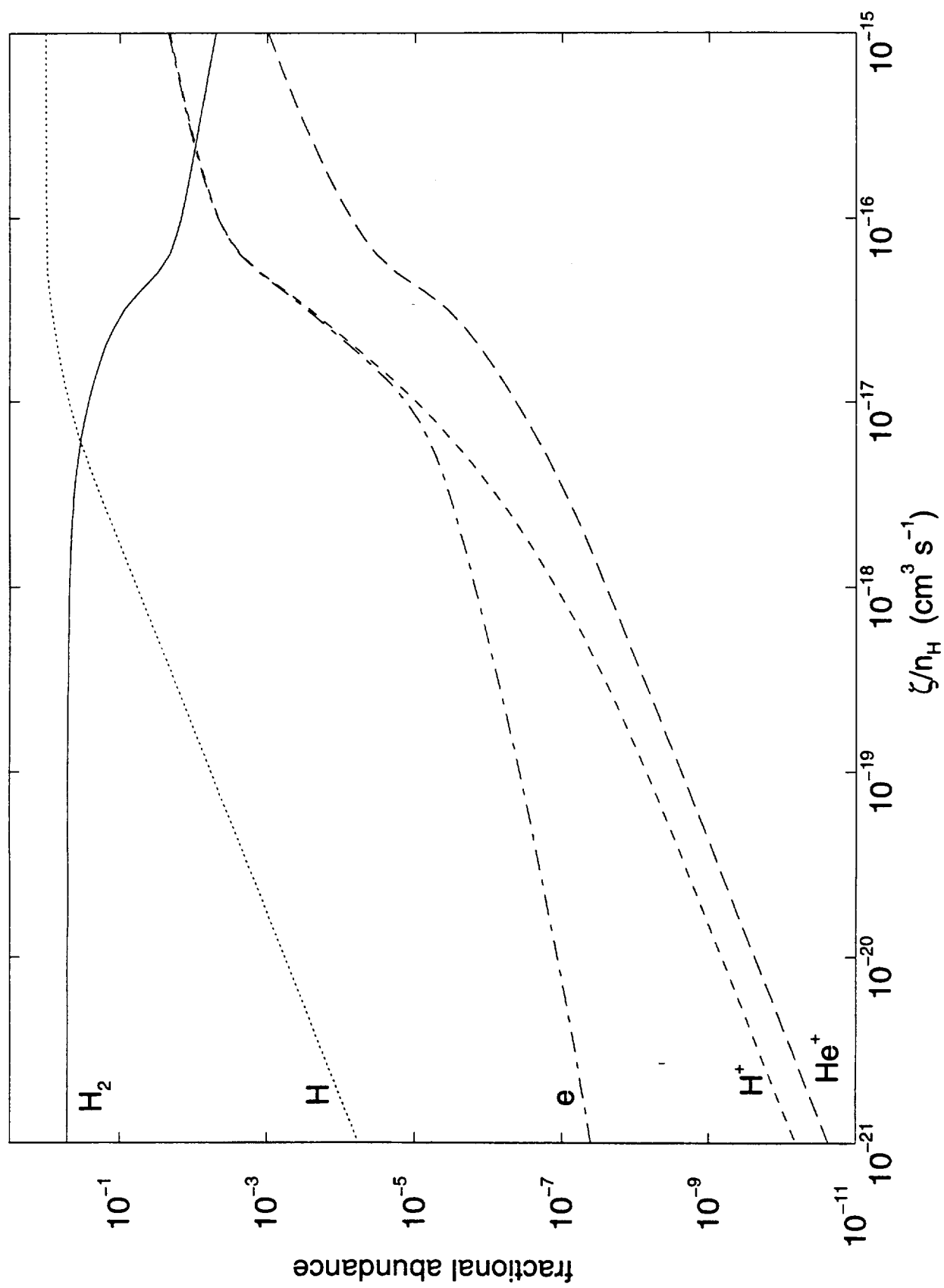
Fig. 3.— H<sub>2</sub> emission spectra produced at  $\zeta/n_H=10^{-17} \text{ cm}^3 \text{ s}^{-1}$  and T=500K with electron pumping either included (top) or excluded (bottom) for a density of (a)  $10 \text{ cm}^{-3}$ , (b)  $10^3 \text{ cm}^{-3}$ , (c)  $10^5 \text{ cm}^{-3}$  and (d)  $10^7 \text{ cm}^{-3}$ .

Fig. 4.— (a)-(c) The ratio 2-1S(1)/1-0S(1) as a function of  $\zeta/n_H$ .

**Fig.1**



**Fig.2**



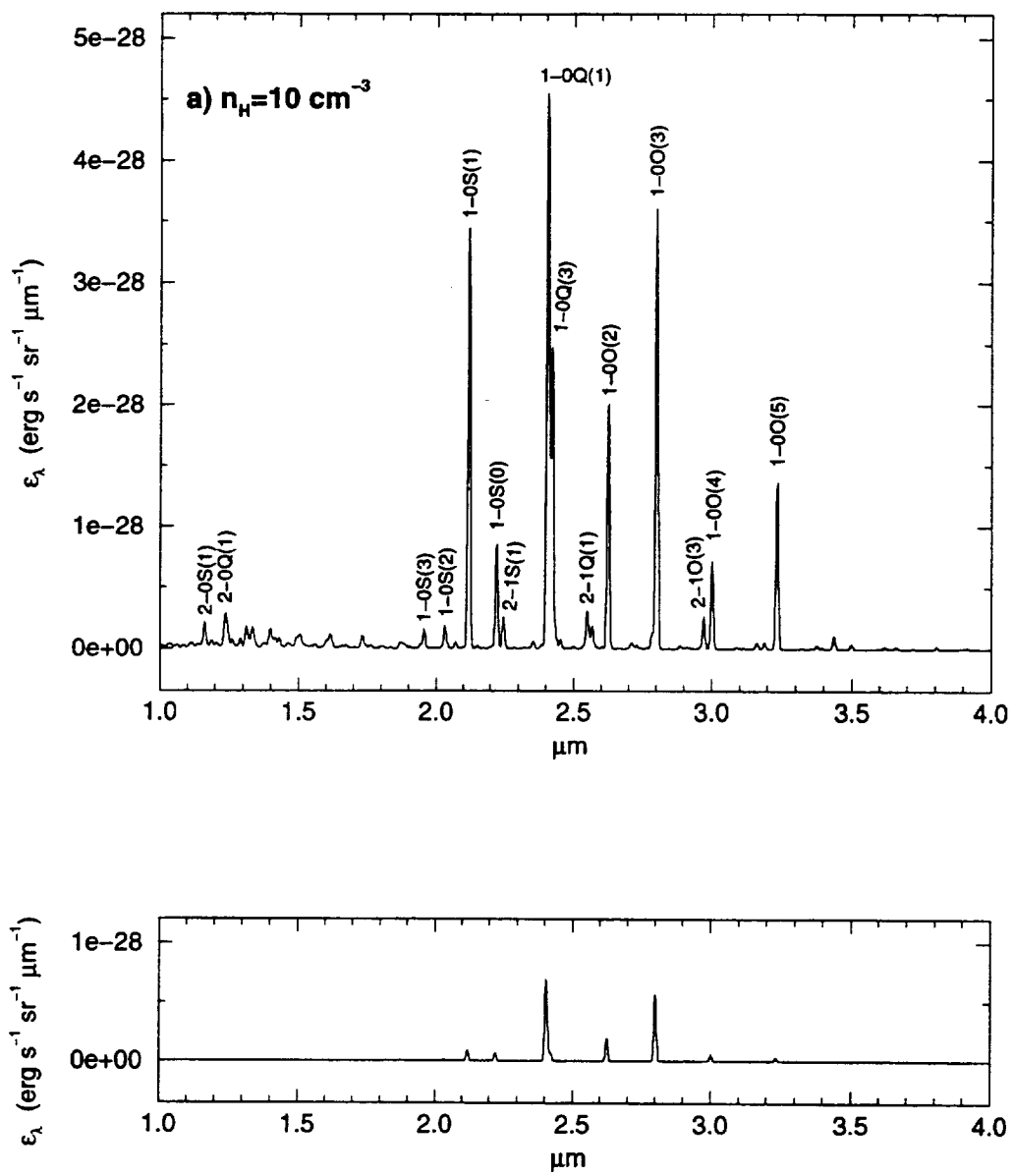


**Fig.3a**

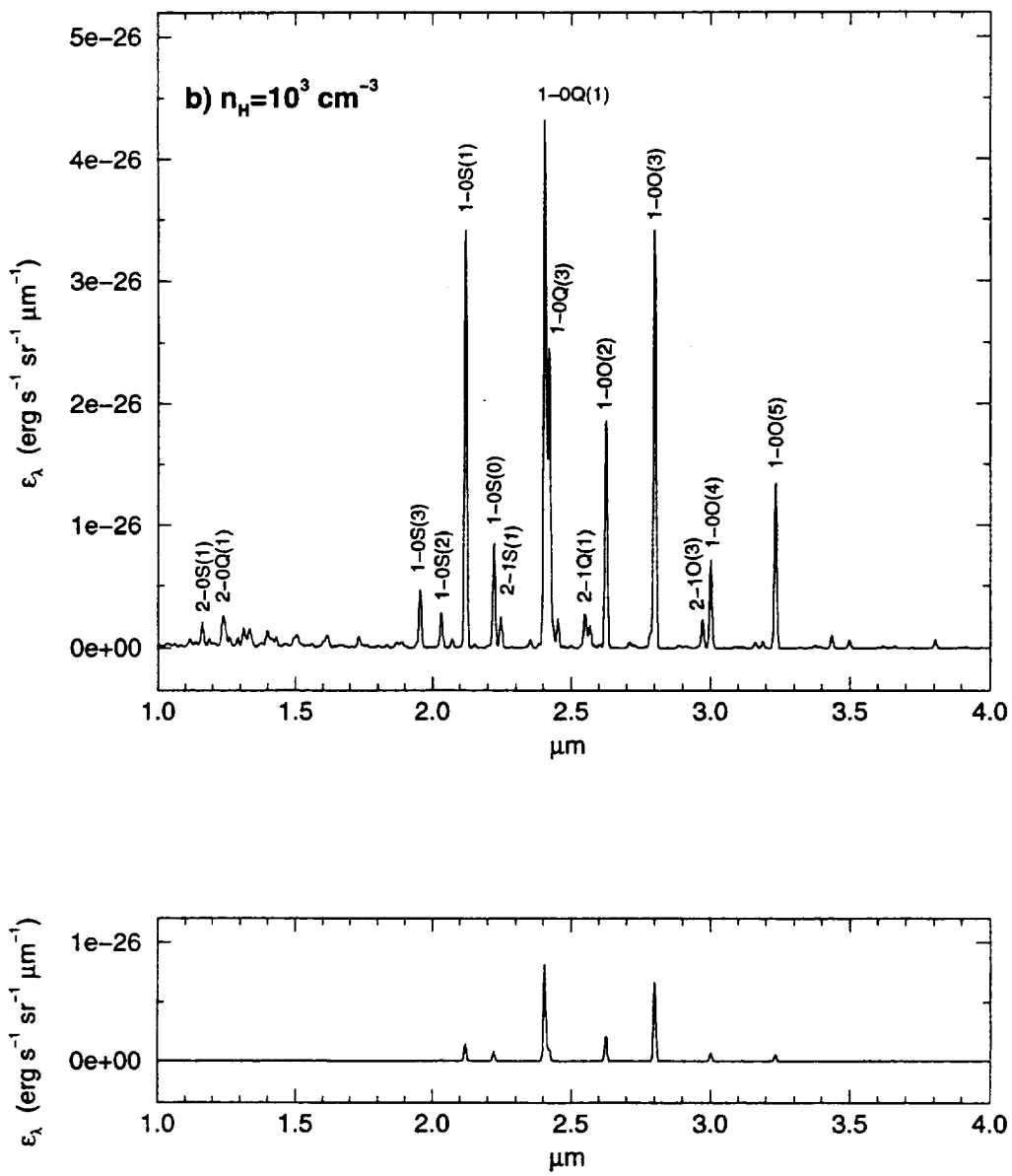


**Fig.3b**

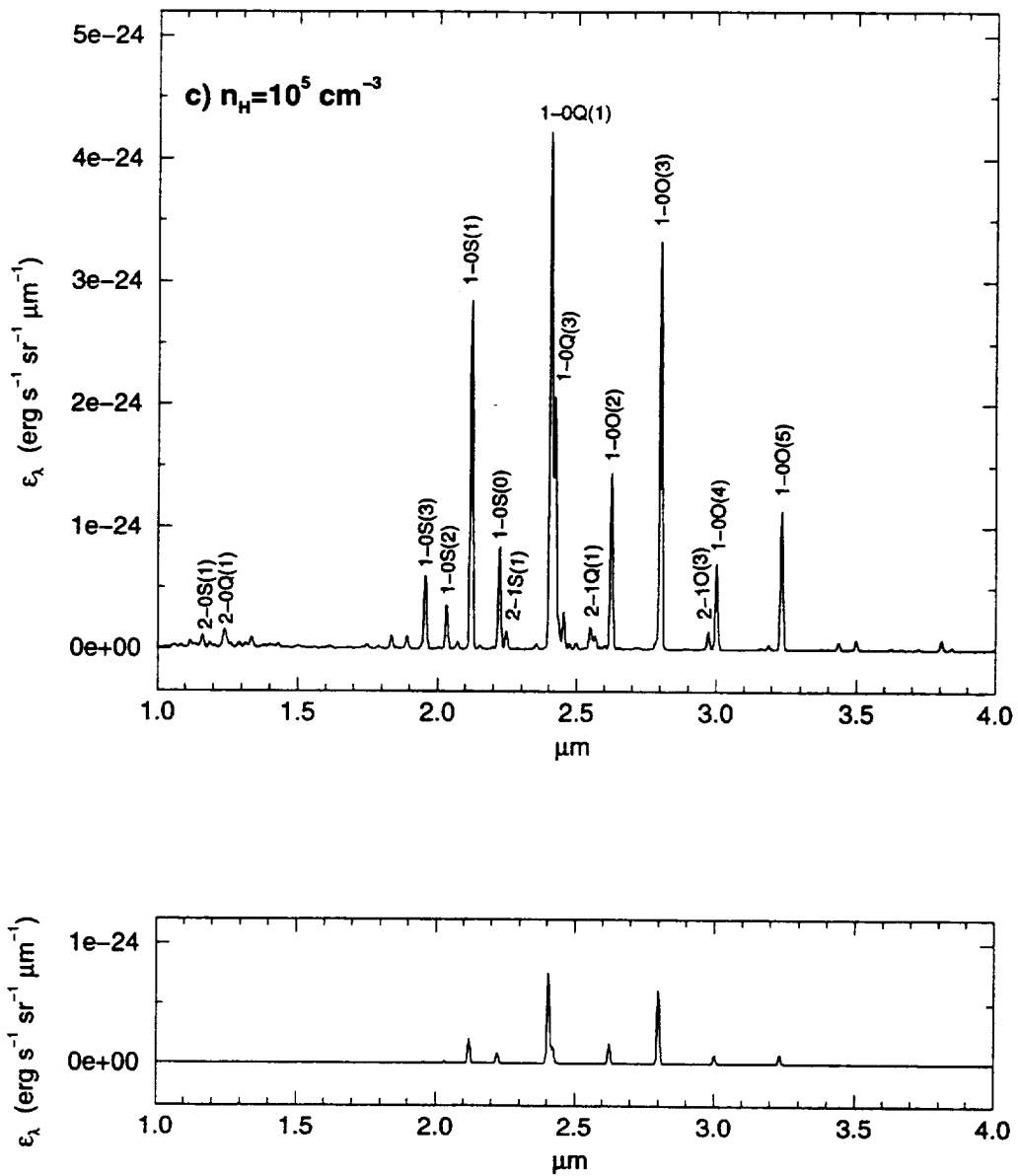


**Fig.3c**

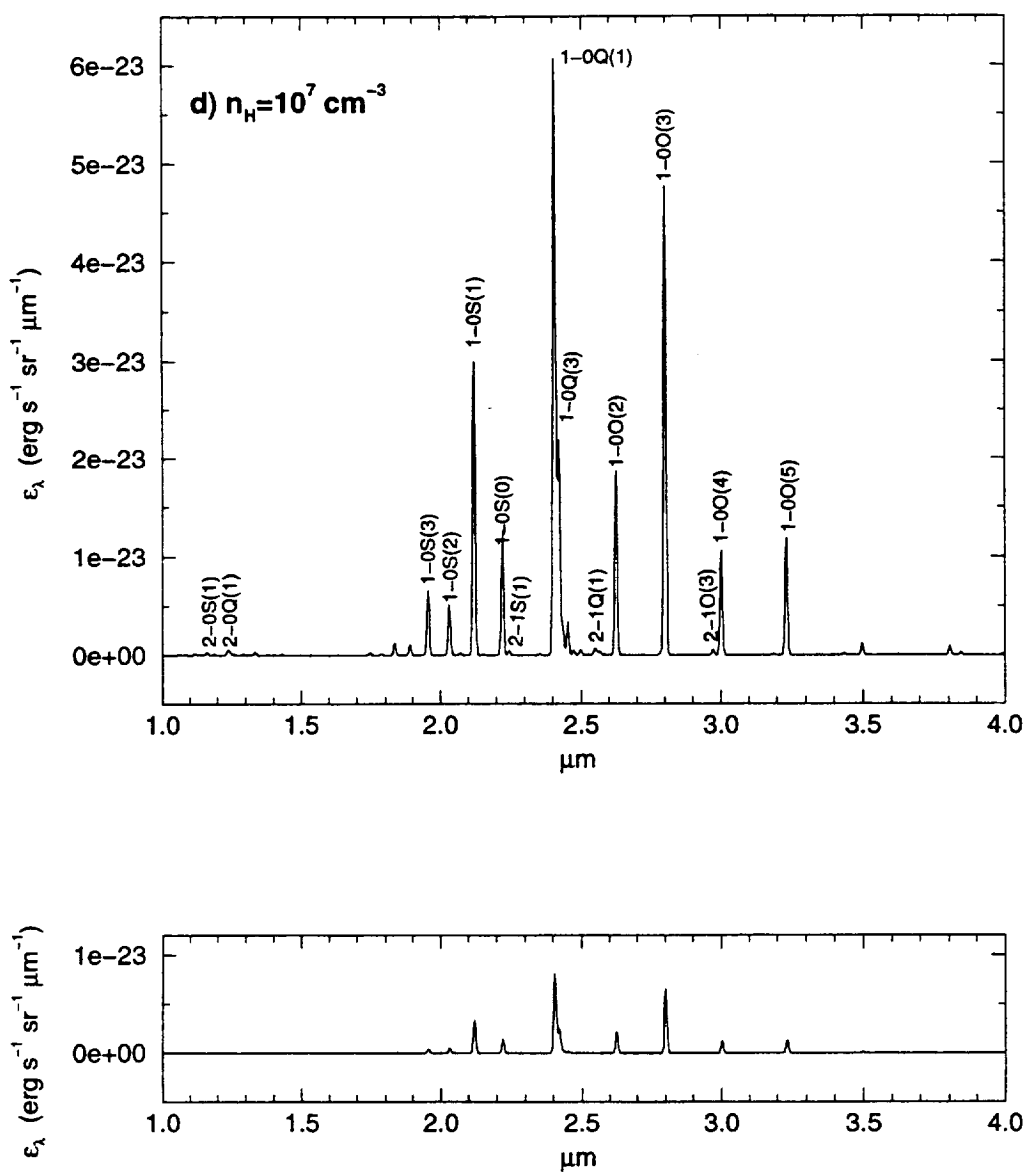
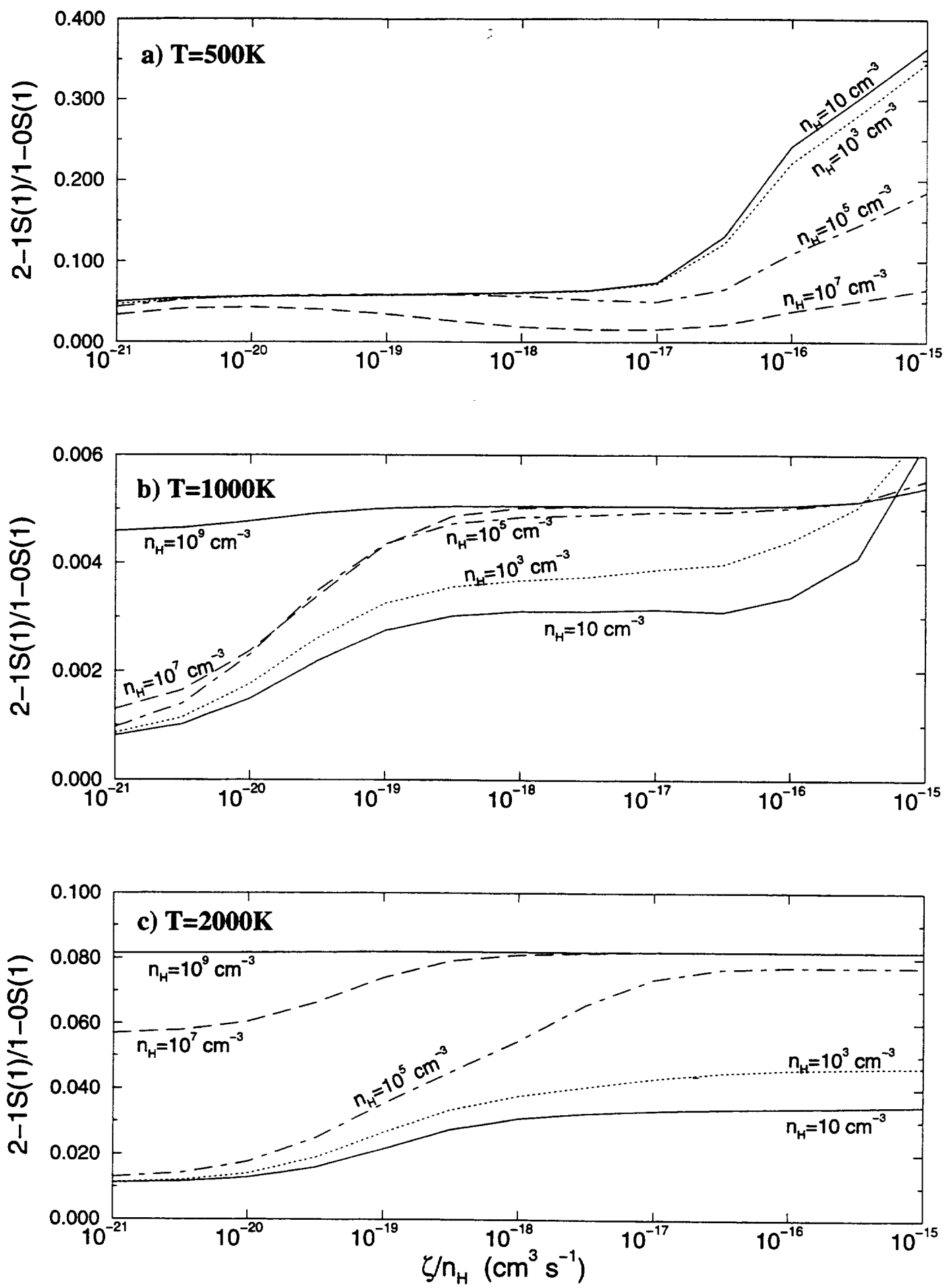


**Fig.3d**

**Fig.4**



$^2\Sigma_u$  symmetry  $R=1.20a_0$

$Q_{\max}$  from 2-state calculations

